Electronic Supplementary Material (ESI) for Dalton Transactions.

Supplementary Material

Effect of substituents on the ability of nickel Schiff base complexes with four pendant groups to bind to G-quadruplexes

Nawal Assadawi,[a] Myles Ferderer,[a] Nicholas Kusi-Appauh,[a] Haibo Yu,[a] Carolyn Dillon,[a] Ron Sluyter,[a] Christopher Richardson[a] and Stephen Ralph[a]

[a] Molecular Horizons and School of Chemistry and Molecular Bioscience, University of Wollongong, Northfields Avenue, Wollongong 2522, Australia

E-mail: sralph@uow.edu.au

Table S1: Crystal data and structure refinement for **(13)** and **(16)**.

Identification code	**(13)** (exp_84Ni20)	**(16)** (exp_219_NA)
Empirical formula	$C_{56}H_{74.41}N_6NiO_{6.21}$	$C_{41}H_{72}N_6NiO_{16.5}$
Formula weight	989.61	966.15
Temperature/K	149.99(10)	150.01(10)
Crystal system	monoclinic	triclinic
Space group	$P2_1/c$	P-1
a/Å	10.7829(3)	9.7651(2)
b/Å	21.9025(5)	14.6637(3)
c/Å	22.2389(5)	16.8916(3)
α/°	90	78.2060(10)
β/°	99.678(3)	83.1790(10)
γ/°	90	89.109(2)
Volume/Å^3	5177.4(2)	2350.83(8)
Z	4	2
ρ_{calc}g/cm^3	1.270	1.365
μ/mm^{-1}	0.431	0.487
F(000)	2120.0	1034.0
Crystal size/mm^3	0.41 × 0.19 × 0.18	0.7 × 0.2 × 0.19
Radiation	Mo Kα (λ = 0.71073Å)	MoKα (λ = 0.71073Å)
2Θ range for data collection/°	4.87 to 56.566	4.132 to 58.26
Index ranges	-12 ≤ h ≤ 14, -28 ≤ k ≤ 29, -28 ≤ l ≤ 29	-13 ≤ h ≤ 13, -20 ≤ k ≤ 20, -23 ≤ l ≤ 23
Reflections collected	39931	104375
Independent reflections	12745 [R_{int} = 0.0398, R_{sigma} = 0.0584]	12431 [R_{int} = 0.0335, R_{sigma} = 0.0178]
Data/restraints/parameters	12745/181/659	12431/80/675
Goodness-of-fit on F^2	1.025	1.035
Final R indexes [I>=2σ (I)]	R_1 = 0.0639, wR_2 = 0.1480	R_1 = 0.0385, wR_2 = 0.1051
Final R indexes [all data]	R_1 = 0.1032, wR_2 = 0.1661	R_1 = 0.0469, wR_2 = 0.1109
Largest diff. peak/hole / e Å^{-3}	0.96/-0.42	0.91/-0.49
CCDC	2327214	2327215

Table S2: Binding free energies obtained from docking studies performed using nickel Schiff base complexes and either 1KF1 or 1KBD.

Complex	1KF1(qDNA)		1KBD (dsDNA)	
	ΔG (kcal/mol)[a]	Binding mode[b]	ΔG (kcal/mol)[a]	Binding mode[b]
(4)	-9.6 ± 0.1	Top, end stacking	-8.8 ± 0.1	Minor groove
(5)	-9.9 ± 0.1	Top, end stacking	-8.8 ± 0.1	Minor groove
(6)	-9.4 ± 0.1	Top, end stacking	-8.3 ± 0.2	Minor groove
(7)	-9.0 ± 0.1	Top, end stacking	-8.4 ± 0.1	Minor groove
(8)	-8.7 ± 0.1	Top, end stacking	-8.6 ± 0.1	Minor groove
(9)	-8.3 ± 0.1	Bottom, end stacking	-8.0 ± 0.1	Minor groove
(10)	-8.6 ± 0.1	Top, end stacking	-8.4 ± 0.1	Minor groove
(11)	-9.0 ± 0.1	Top, end stacking	-8.4 ± 0.1	Minor groove
(12)	-8.6 ± 0.1	Bottom, end stacking	-8.1 ± 0.1	Minor groove
(13)	-8.6 ± 0.1	Bottom, end stacking	-8.4 ± 0.1	Minor groove
(14)	-8.8 ± 0.1	Top, groove	-8.5 ± 0.1	Minor groove
(15)	-9.1 ± 0.1	Top, end stacking	-8.7 ± 0.1	Minor groove
(16)	-9.2 ± 0.1	Top, groove	-8.9 ± 0.1	Minor groove
(17)	-8.9 ± 0.1	Top, groove	-8.3 ± 0.1	Minor groove

[a] Average values of ΔG with standard errors obtained from the top five docking scores.

[b] "Top" or "Bottom" indicates which terminal G-tetrad was the preferred binding site.

Table S3: IC_{50} values derived from MTT assays performed using THP-1 leukemia cells and different nickel Schiff base complexes.

Complex	IC_{50} (μM)[a]
(18)	10.6 ± 2.0
(19)	3.1 ± 0.7
(21)	5.1 ± 1.3
(22)	10.0 ± 0.2

[a] Error bars represent standard error of the mean for n = 3.

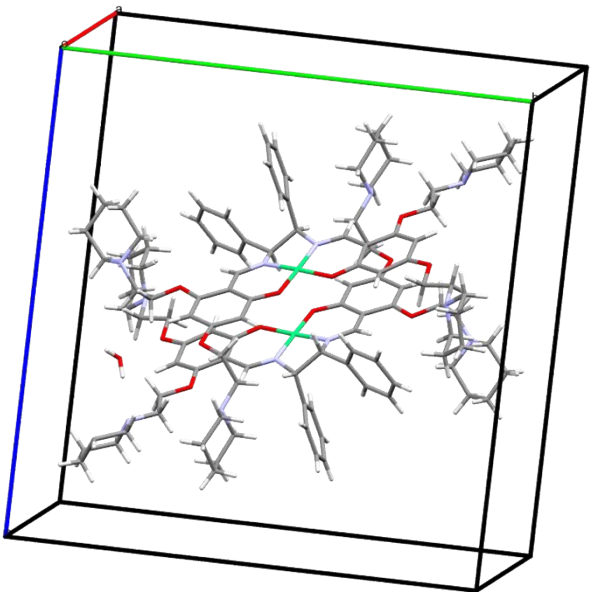

(a)

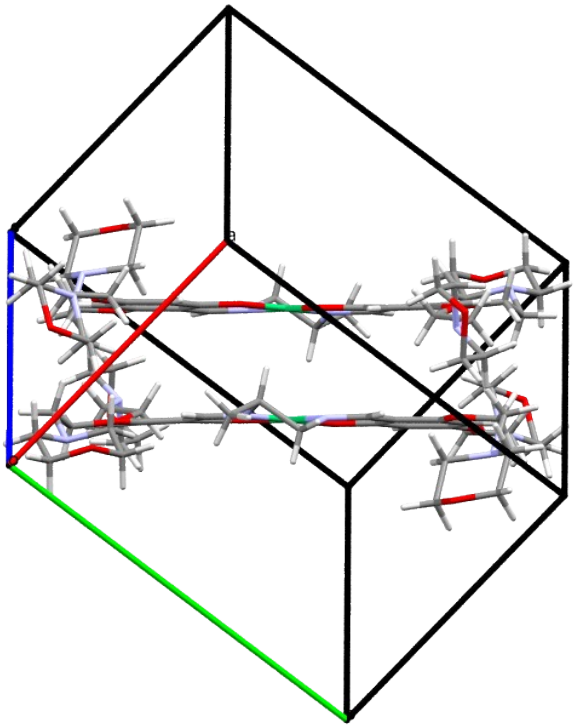

(b)

Figure S1: Arrangement of the nickel molecules in the solid-state structures of **(13)** and **(16)**: (a) Complex **(13)**. (b) Complex **(16)**.

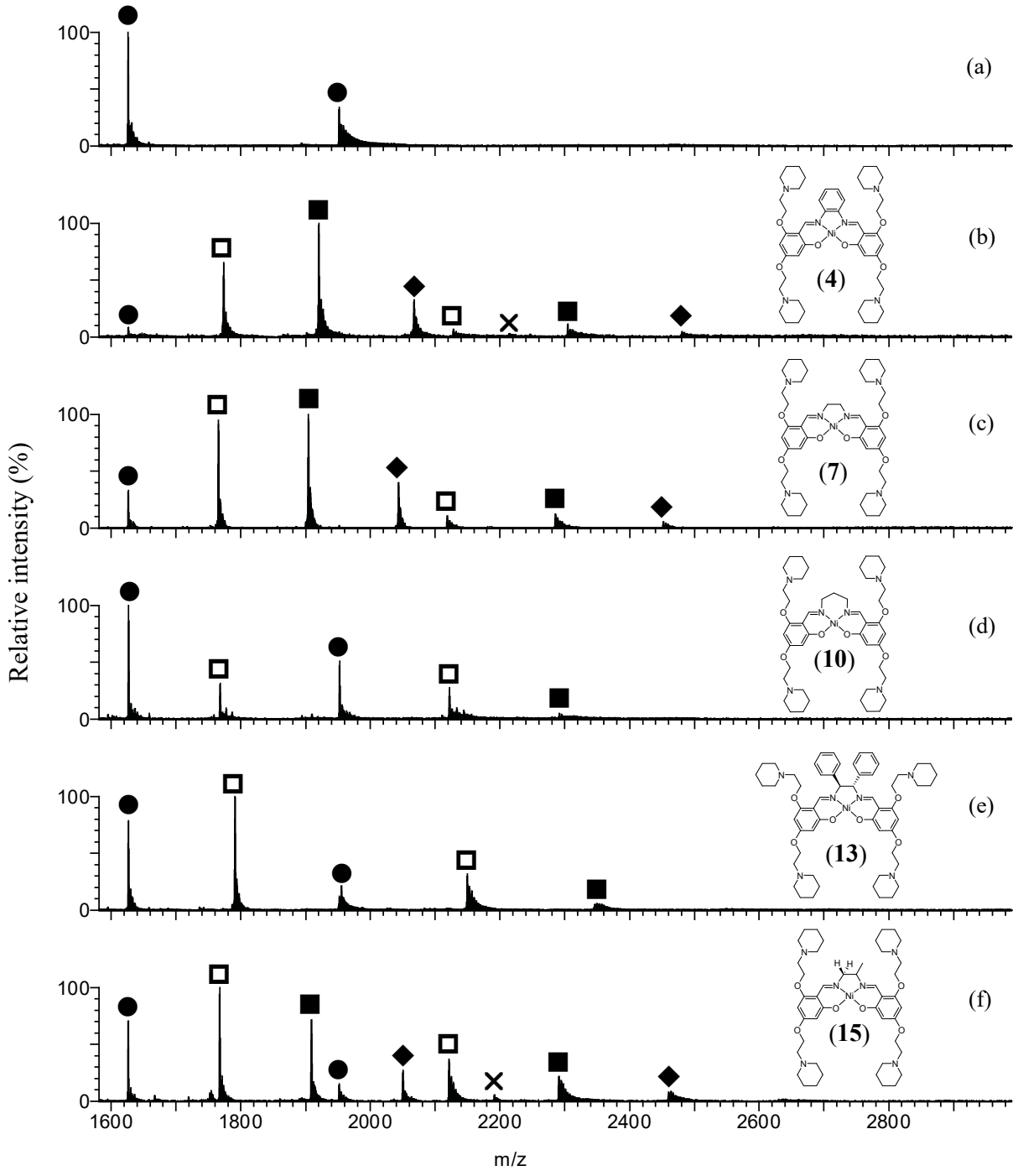

Figure S2: Negative ion ESI mass spectra of solutions containing a 6:1 ratio of different nickel Schiff base complexes and D2: (a) D2 only; (b) D2 + **(4)**; (c) D2 + **(7)**; (d) D2 + **(10)**; (e) D2 + **(15)** and (f) D2 + **(13)**. ● = Free D2; ☐ = [D2 + 1(Ni)]; ■ = [D2 + 2(Ni)]; ◆ = [D2 + 3(Ni)]; ✕ = [D2 + 4(Ni)].

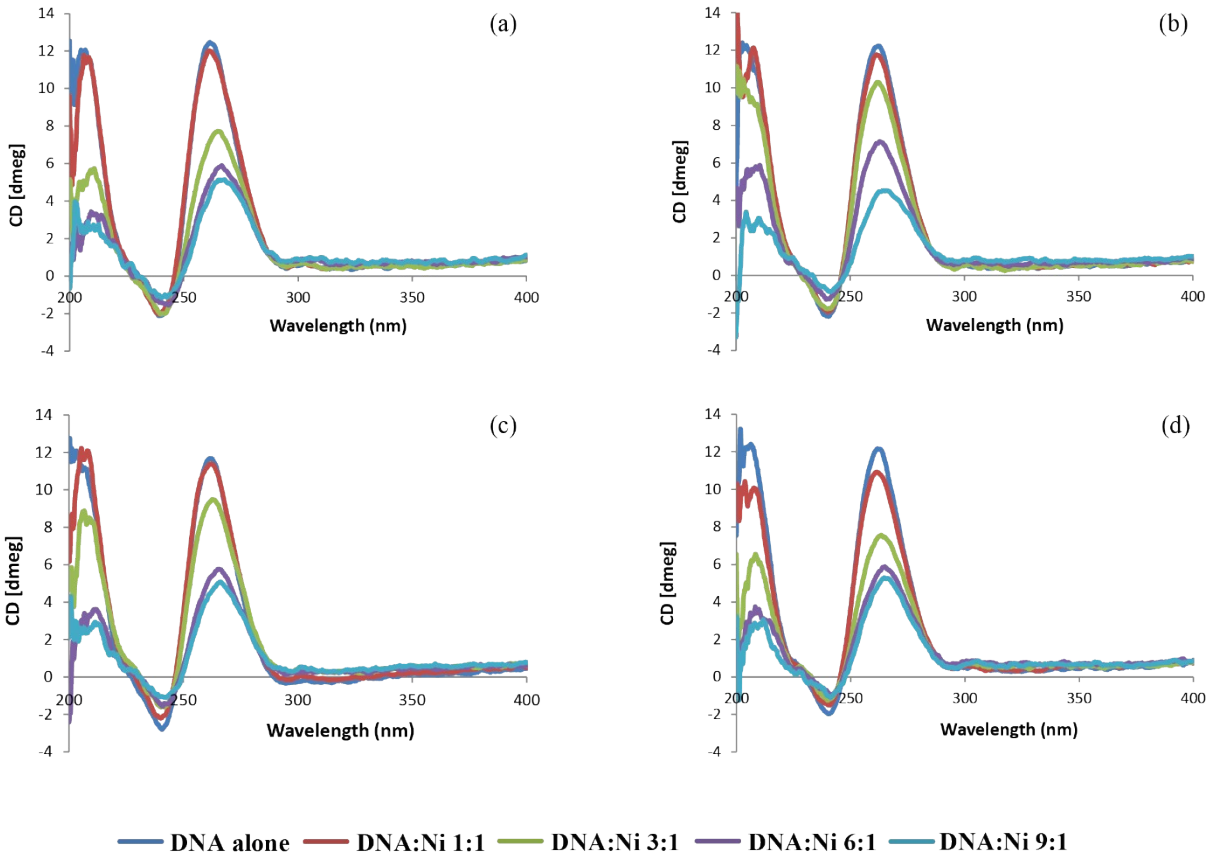

Figure S3: Circular dichroism spectra (200-400 nm) of solutions containing different ratios of nickel Schiff base complexes and *c-kit1*: (a) *c-kit1*+ (**7**); (b) *c-kit1*+ (**10**); (c) *c-kit1*+ (**13**) and (d) *c-kit1*+ (**15**).

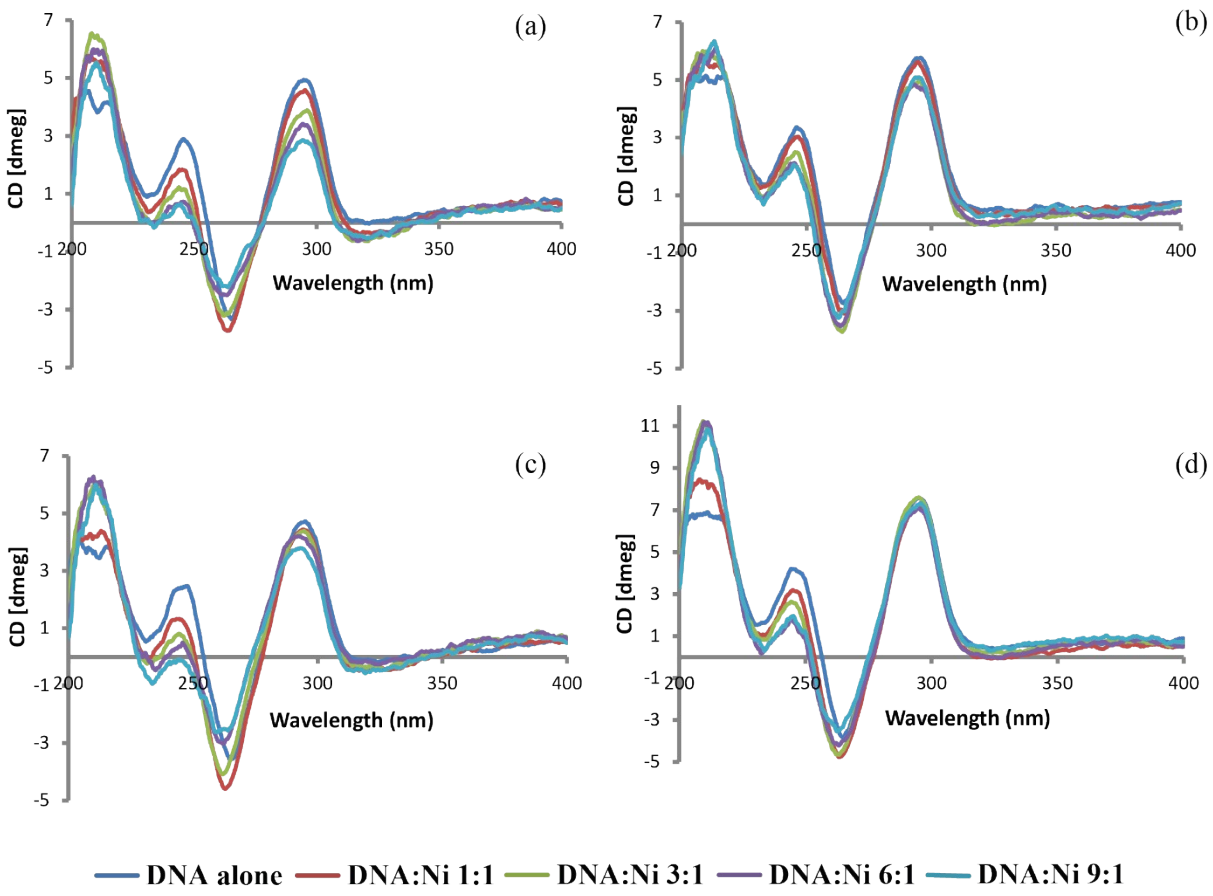

Figure S4: Circular dichroism spectra (200-400 nm) of solutions containing different ratios of nickel Schiff base complexes and anti-parallel Q1: (a) Q1 + (**7**); (b) Q1 + (**10**); (c) Q1 + (**13**) and (d) Q1 + (**15**).

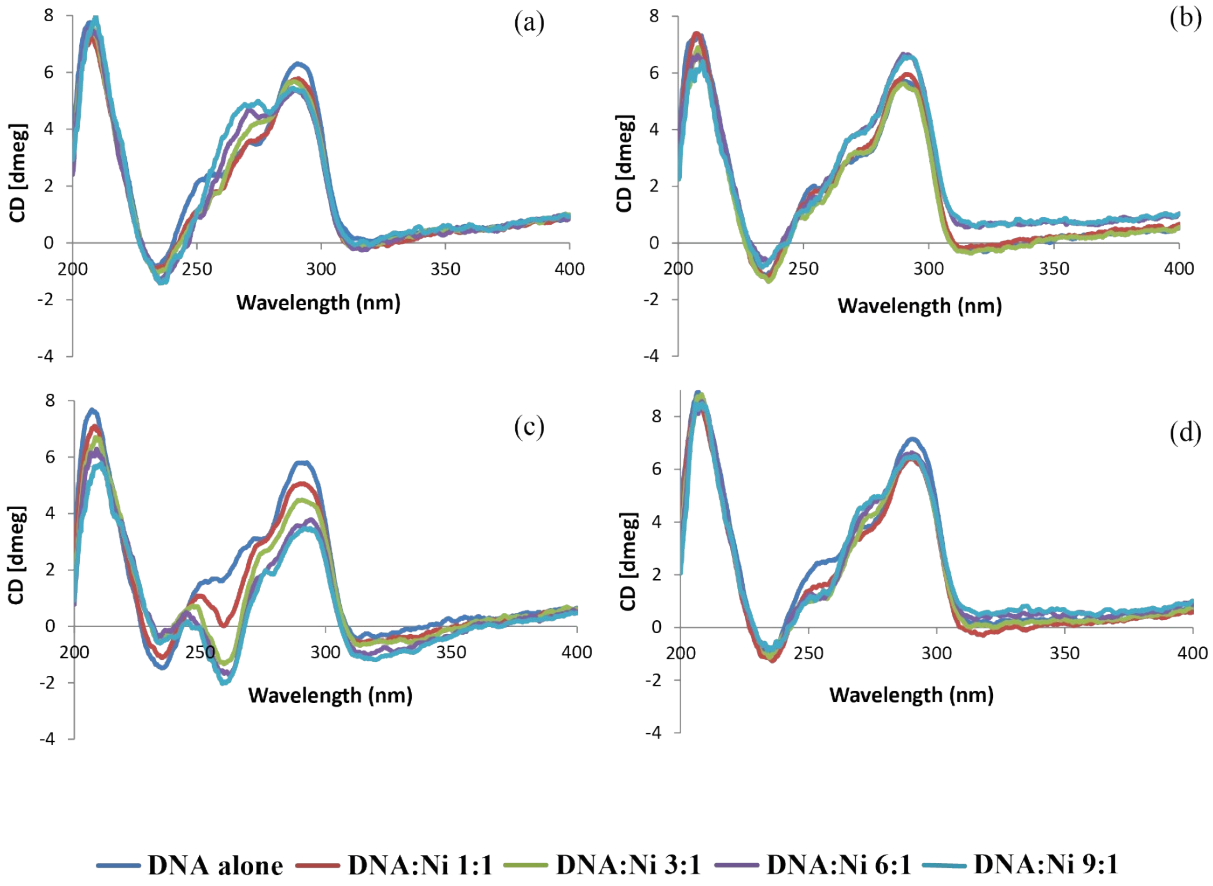

Figure S5: Circular dichroism spectra (200-400 nm) of solutions containing different ratios of nickel Schiff base complexes and hybrid Q1: (a) Q1 + (**7**); (b) Q1 + (**10**); (c) Q1 + (**13**) and (d) Q1 + (**15**).

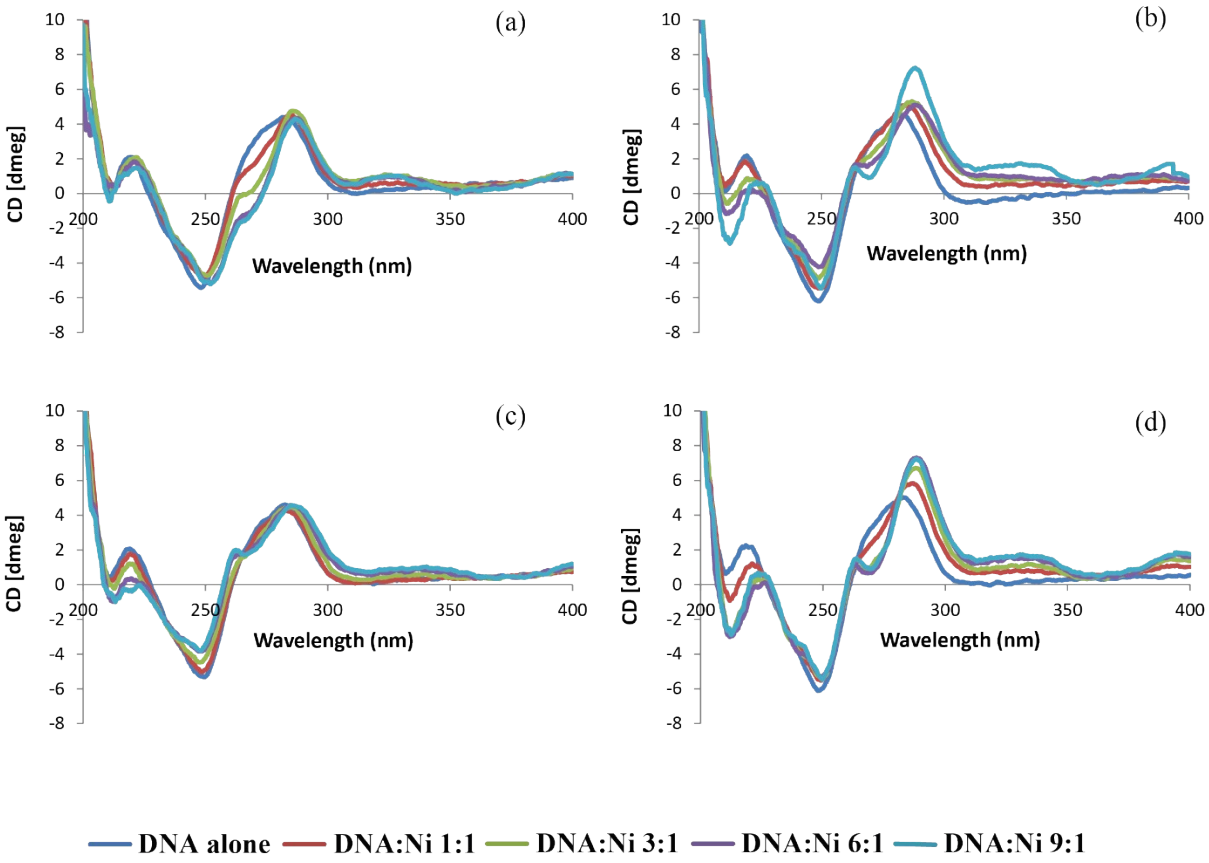

Figure S6: Circular dichroism spectra (200-400 nm) of solutions containing different ratios of nickel Schiff base complexes and D2: (a) D2 + (**7**); (b) D2 + (**10**); (c) D2 + (**13**) and (d) D2 + (**15**).

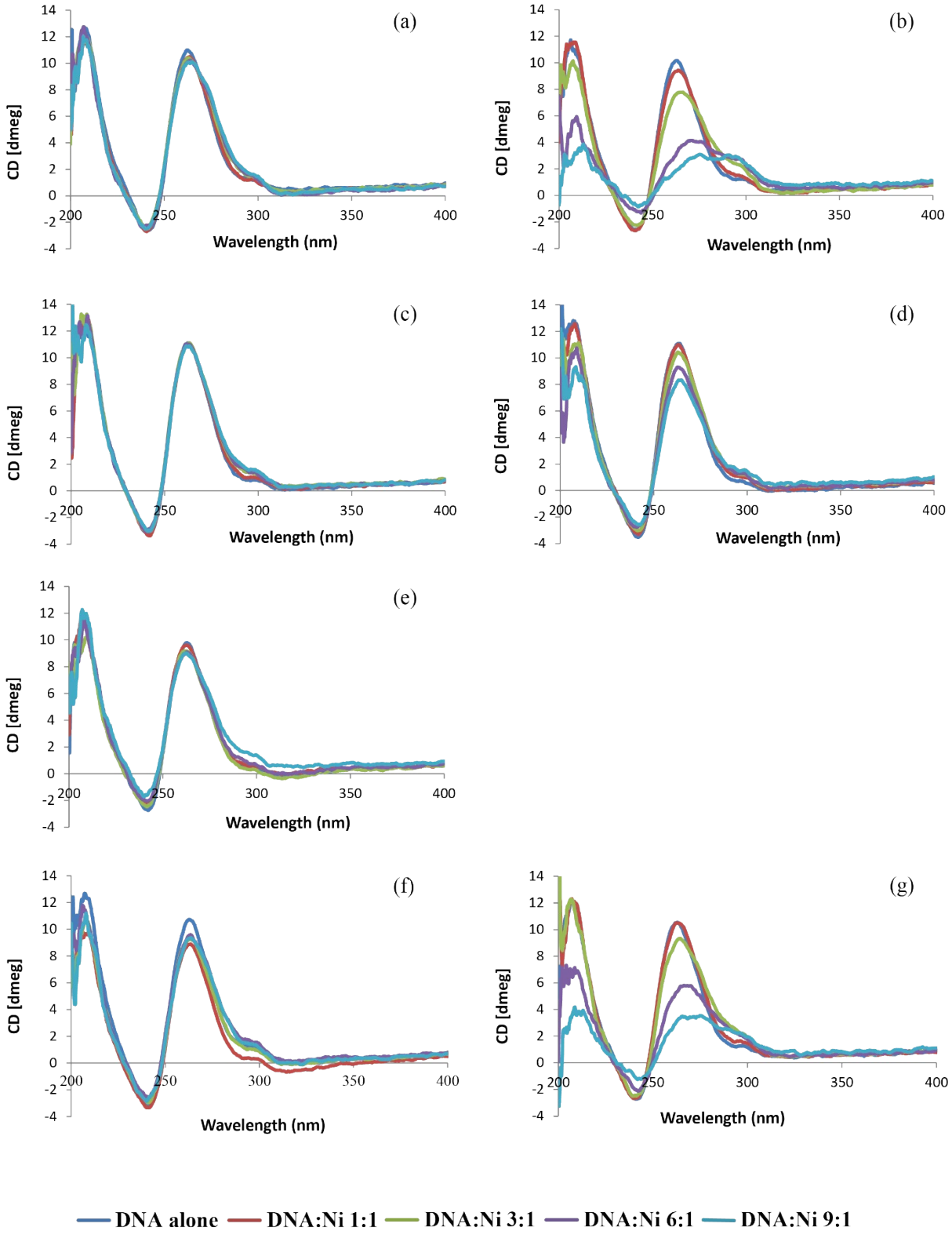

Figure S7: Circular dichroism spectra (200-400 nm) of solutions containing different ratios of nickel Schiff base complexes and parallel Q1: (a) parallel Q1+ **(8)**; (b) parallel Q1+ **(9)**; (c) parallel Q1+ **(11)**; (d) parallel Q1+ **(12)**; (e) parallel Q1+ (**14**); (f) parallel Q1+ (**16**) and (g) parallel Q1+ (**17**).

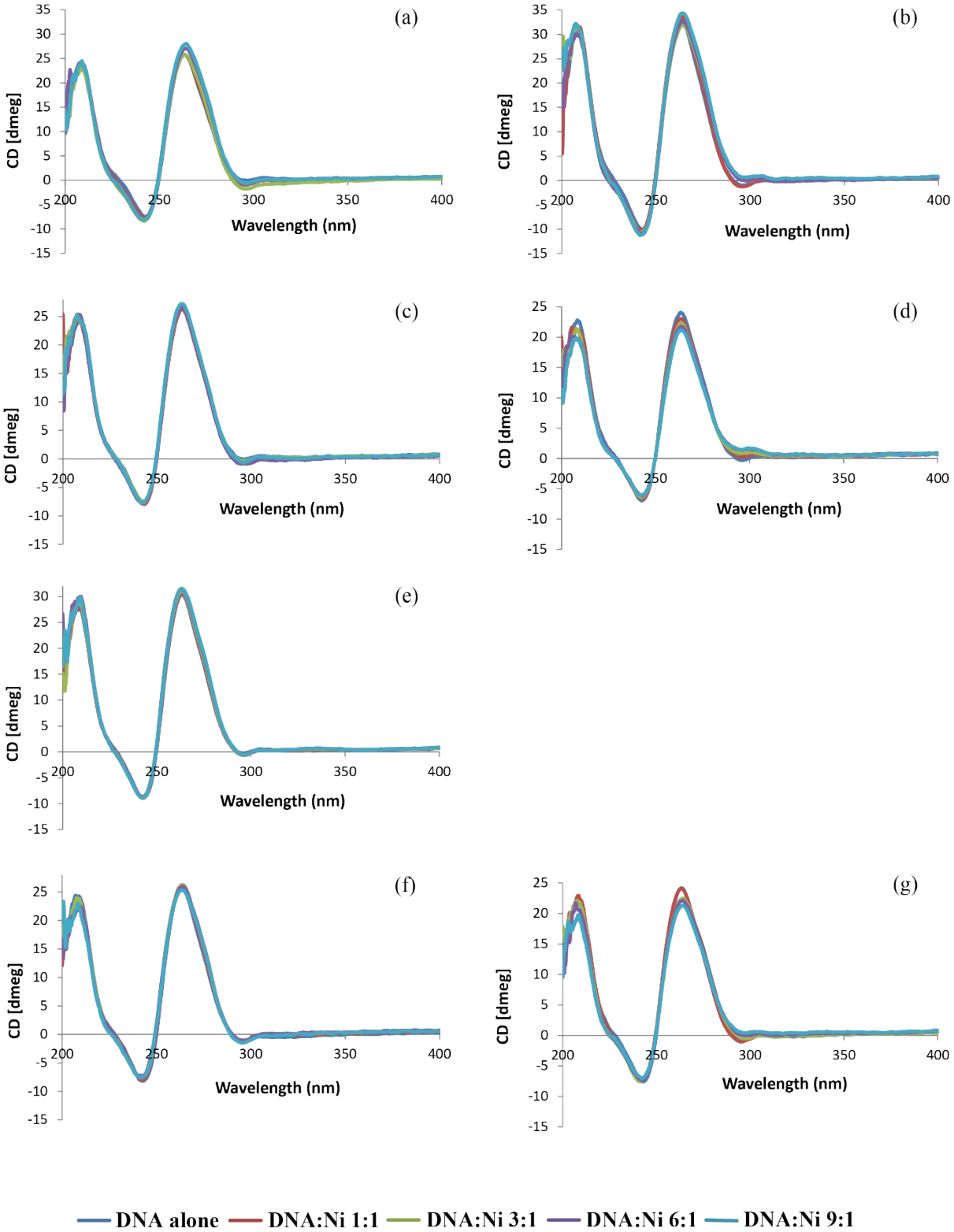

Figure S8: Circular dichroism spectra (200-400 nm) of solutions containing different ratios of nickel Schiff base complexes and parallel Q4: (a) parallel Q4+ **(8)**; (b) parallel Q4+ **(9)**; (c) parallel Q4+ **(11)**; (d) parallel Q4+ **(12)**; (e) parallel Q4+ (**14**); (f) parallel Q4+ (**16**) and (g) parallel Q4+ (**17**).

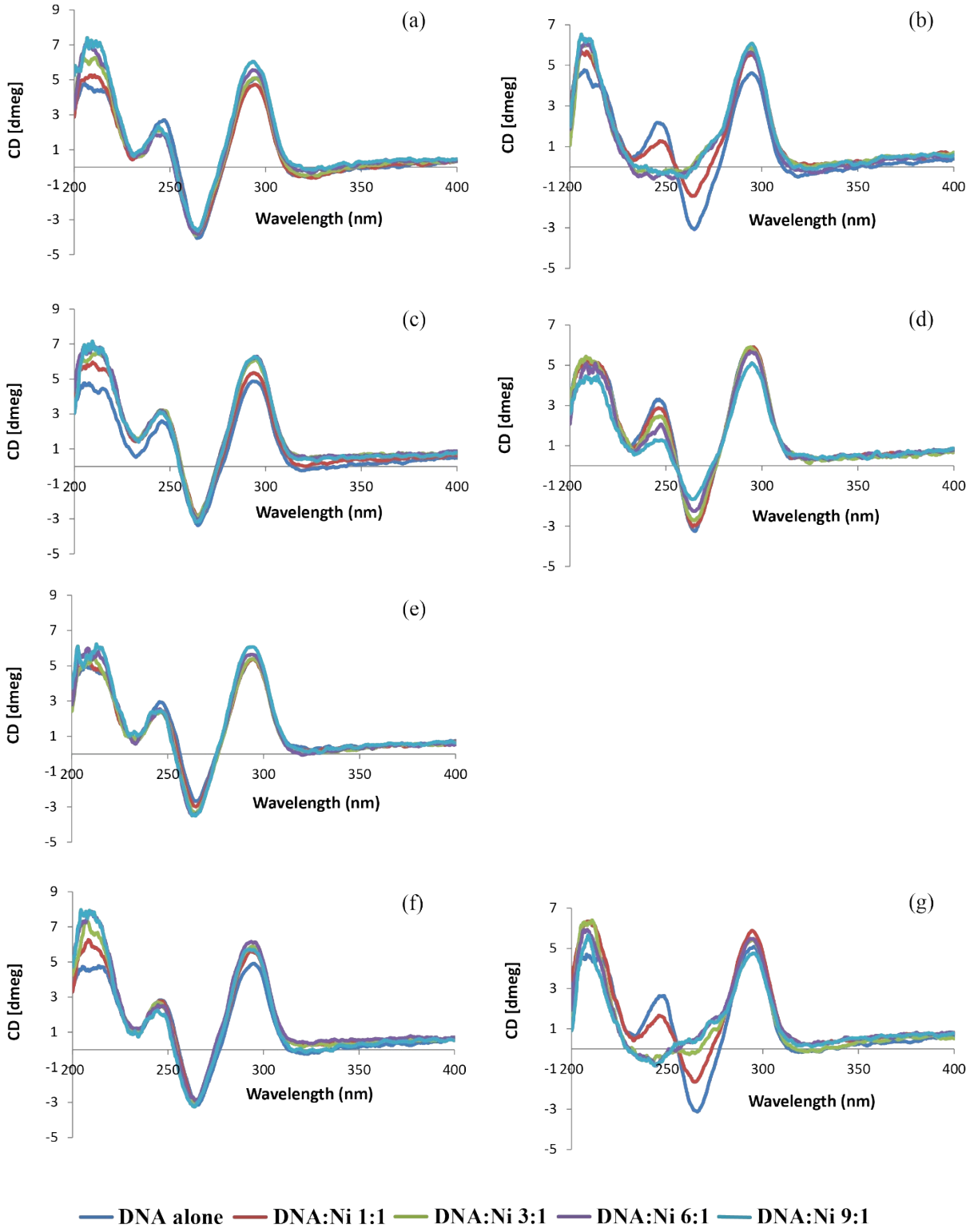

Figure S9: Circular dichroism spectra (200-400 nm) of solutions containing different ratios of nickel Schiff base complexes and anti-parallel Q1: (a) anti-parallel Q1+ **(8)**; (b) anti-parallel Q1+ **(9)**; (c) anti-parallel Q1+ **(11)**; (d) anti-parallel Q1+ **(12)**; (e) anti-parallel Q1+ (**14**); (f) anti-parallel Q1+ (**16**) and (g) anti-parallel Q1+ (**17**).

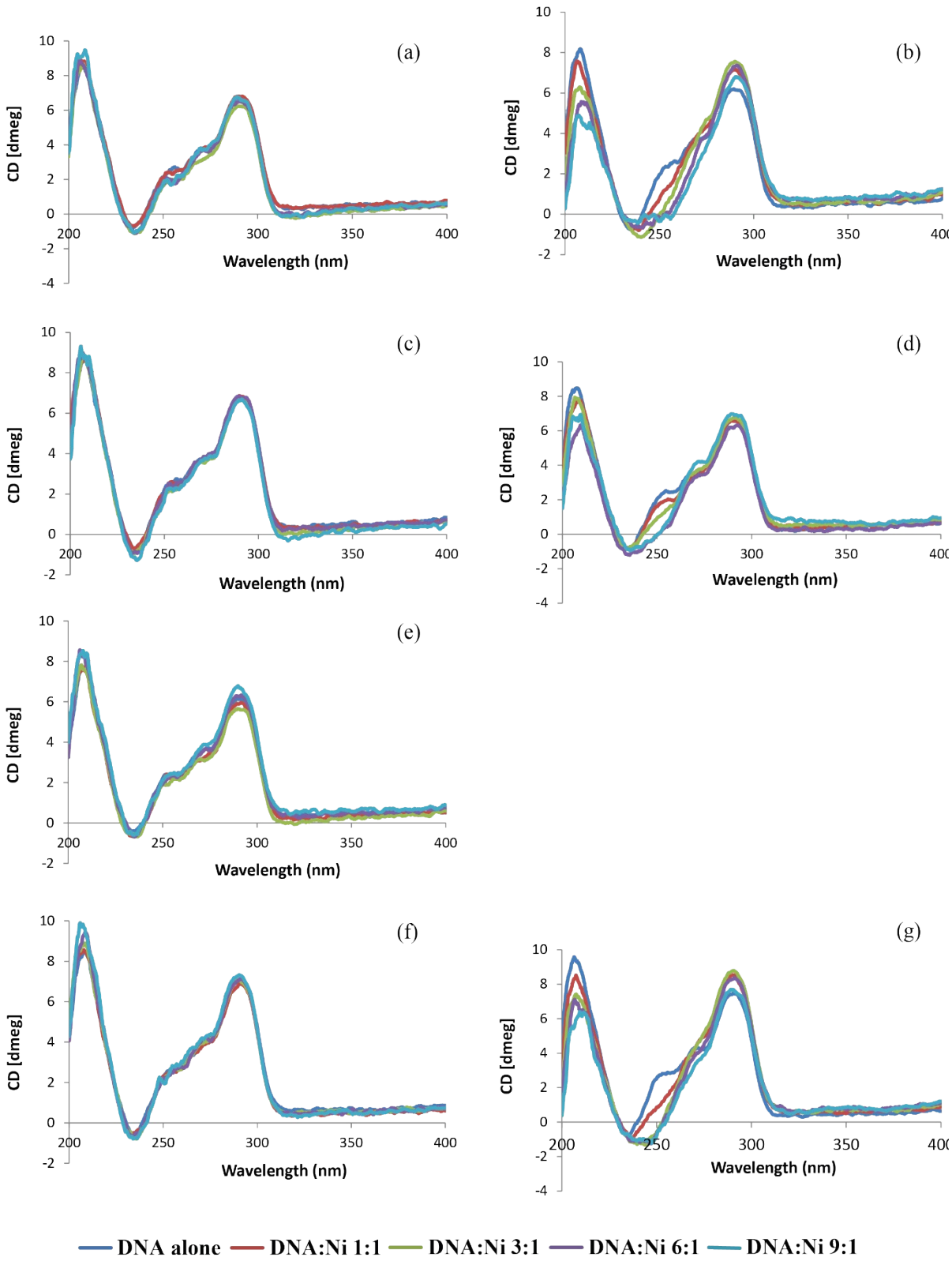

Figure S10: Circular dichroism spectra (200-400 nm) of solutions containing different ratios of nickel Schiff base complexes and hybrid Q1: (a) hybrid Q1+ **(8)**; (b) hybrid Q1+ **(9)**; (c) hybrid Q1+ **(11)**; (d) hybrid Q1+ **(12)**; (e) hybrid Q1+ (**14**); (f) hybrid Q1+ (**16**) and (g) hybrid Q1+ (**17**).

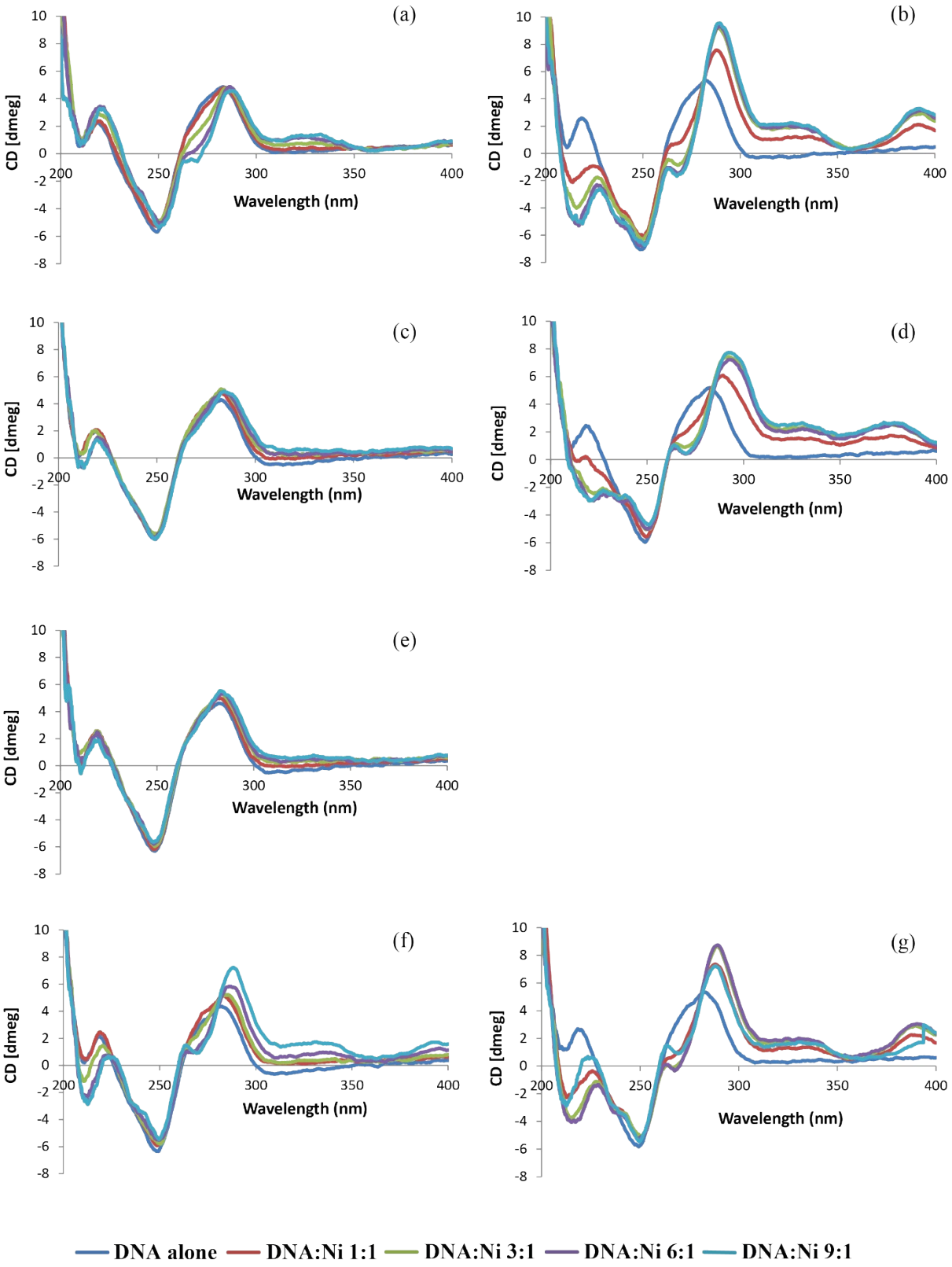

Figure S11: Circular dichroism spectra (200-400 nm) of solutions containing different ratios of nickel Schiff base complexes and D2: (a) D2 + **(8)**; (b) D2 + **(9)**; (c) D2 + **(11)**; (d) D2 + **(12)**; (e) D2 + (**14**); (f) D2 + (**16**) and (g) D2 + (**17**).

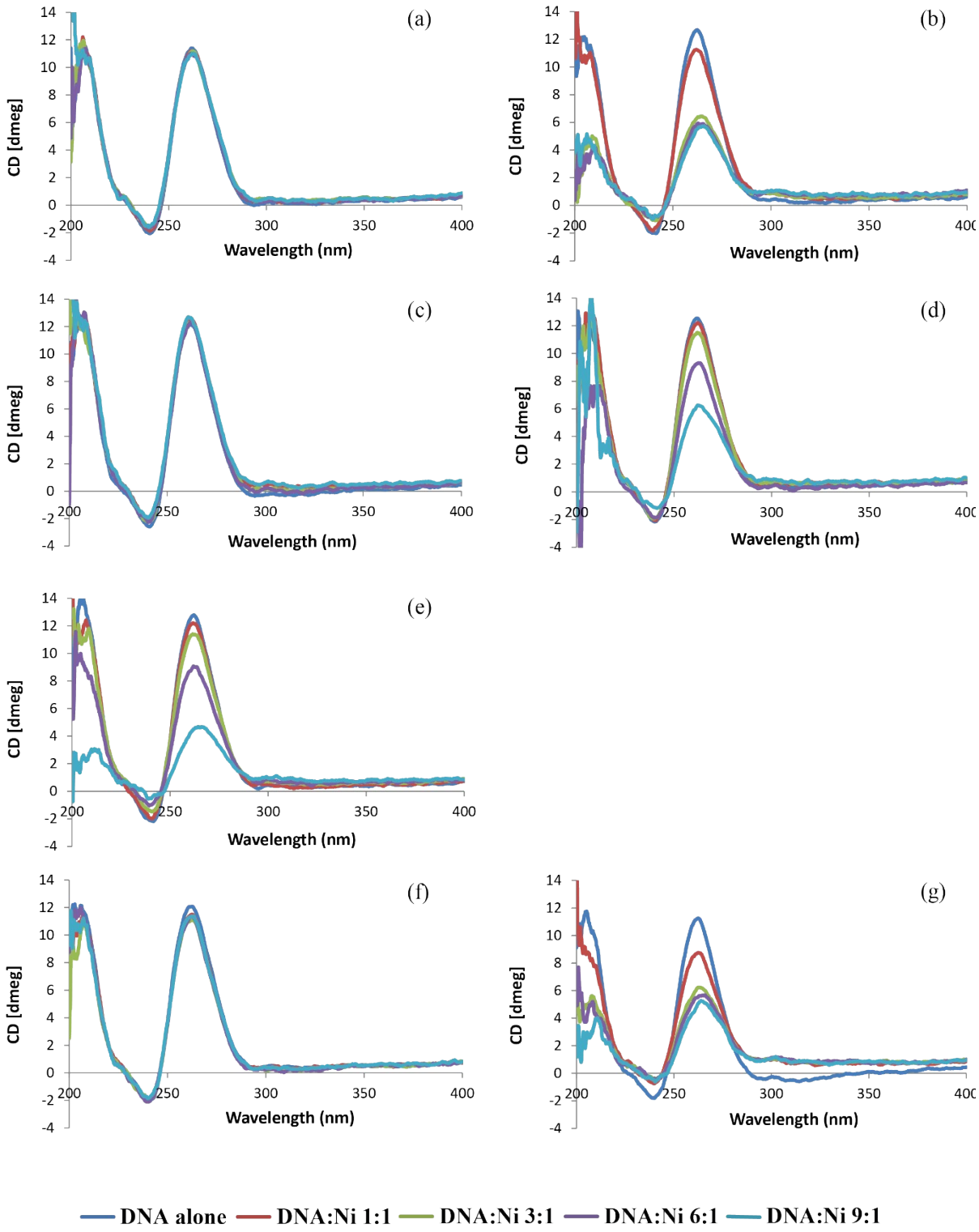

Figure S12: Circular dichroism spectra (200-400 nm) of solutions containing different ratios of nickel Schiff base complexes and C-KIT1: (a) C-KIT1+ **(8)**; (b) C-KIT1+ **(9)**; (c) C-KIT1+ **(11)**; (d) C-KIT1+ **(12)**; (e) C-KIT1+ (**14**); (f) C-KIT1+ (**16**) and (g) C-KIT1+ (**17**).

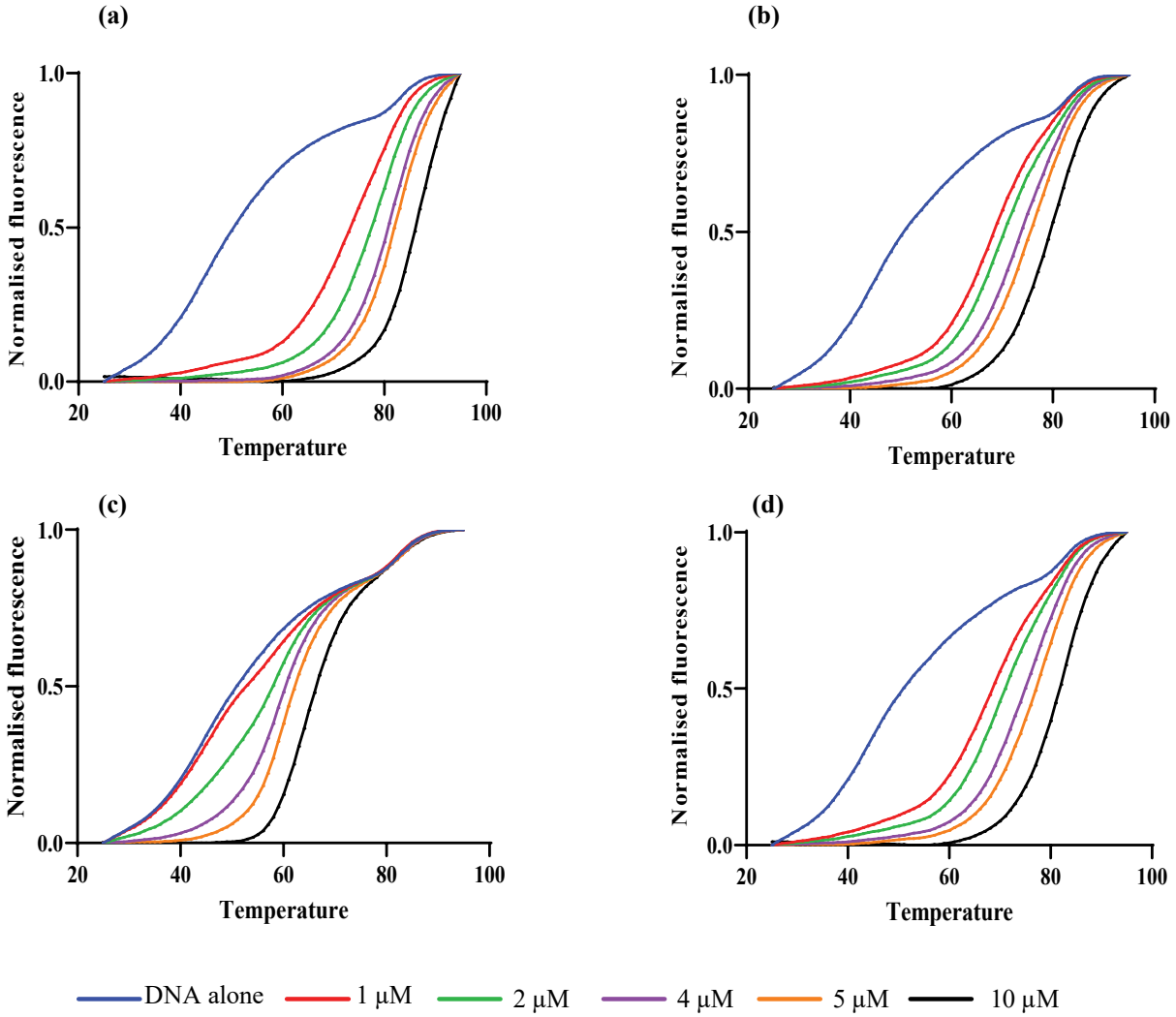

Figure S13: Results obtained from FRET melting assays performed using anti-parallel F21T and increasing concentrations of nickel Schiff base complexes. (a) (**7**); (b) (**10**); (c) (**13**) and (d) (**15**).

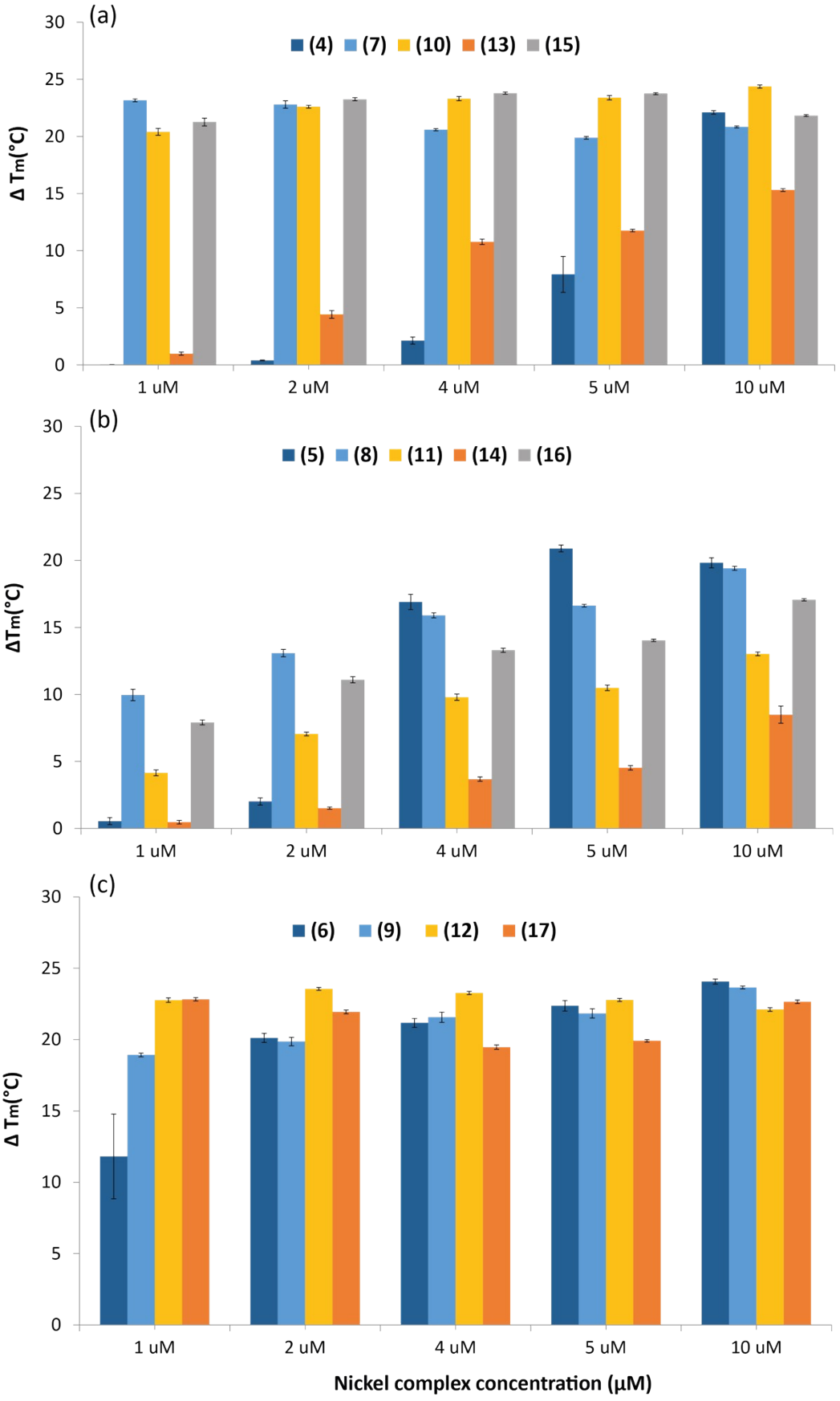

Figure S14: Effect of nickel complexes on ΔT_m for solutions containing 0.20 μM hybrid F21T.

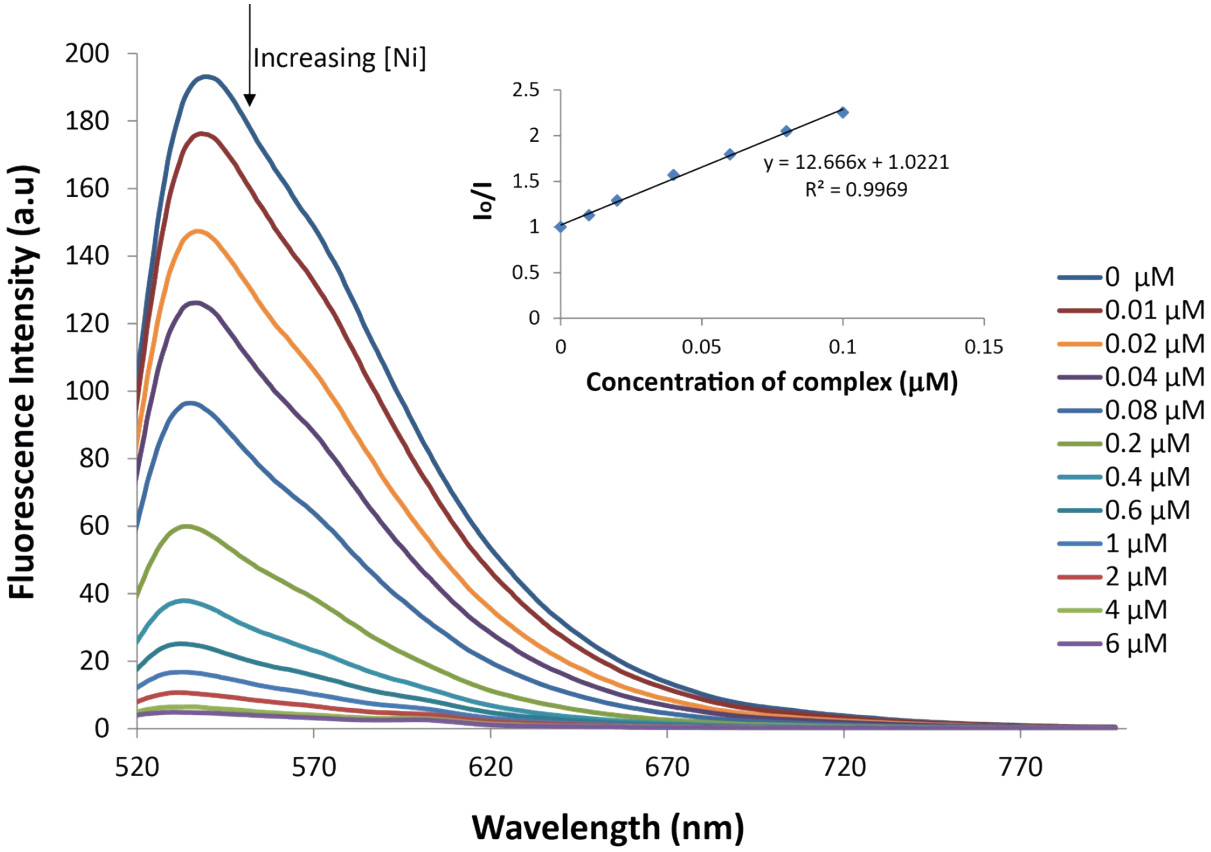

Figure S15: Results from an FID assay performed by adding increasing amounts of (**9**) to a solution containing thiazole orange and parallel Q1. The inset shows a Stern-Volmer plot derived from the data, which was then used to determine the DC_{50} for the nickel complex.

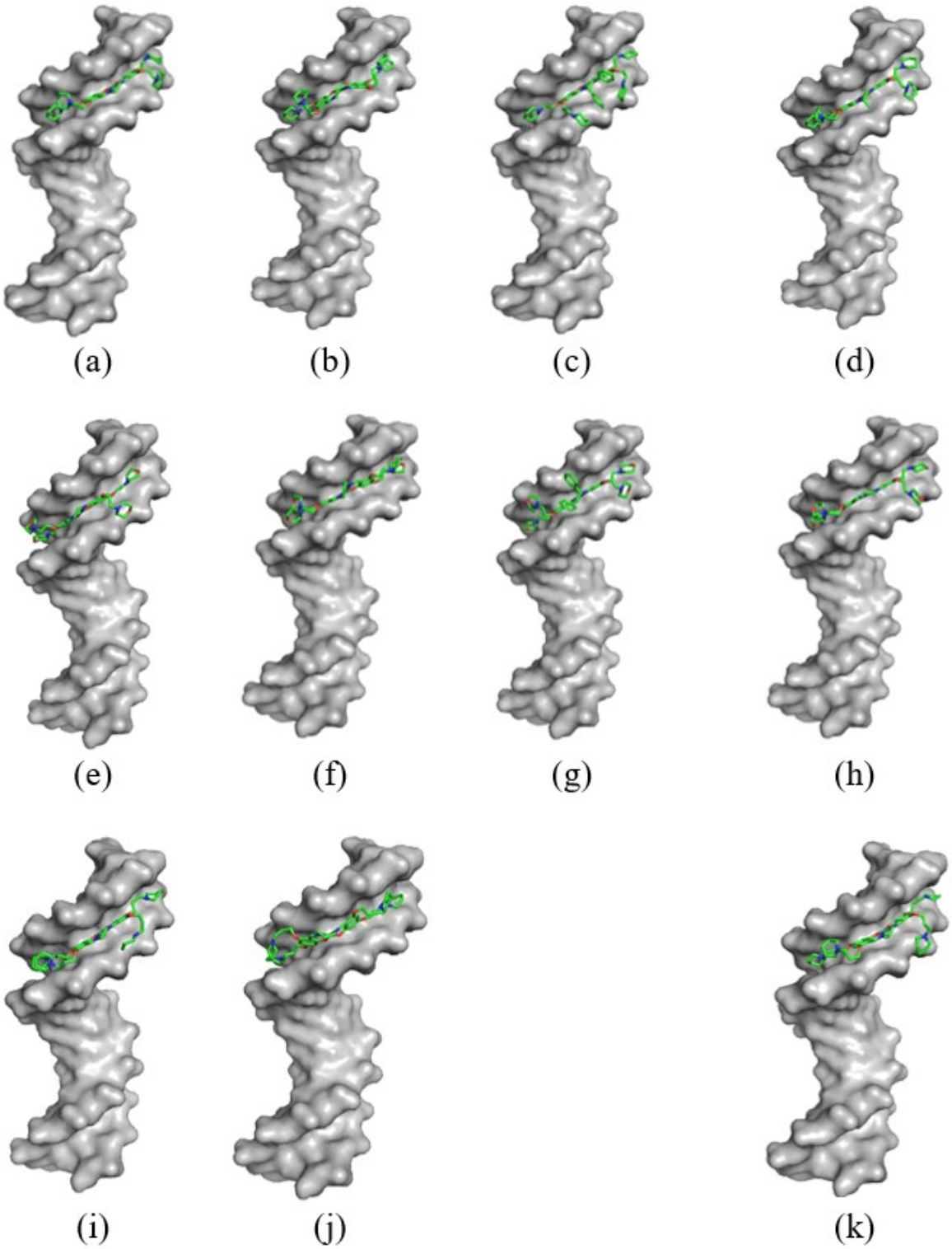

Figure S16: Results from molecular docking experiments performed using the dsDNA 1KBD and different nickel complexes: (a) **(7)**; (b) **(10)**; (c) **(13)**: (d) **(15)**; (e) **(8)**; (f) **(11)**; (g) **(14)**; (h) **(16)**; (i) **(9)**; (j) **(12)** and (k) **(17)**.

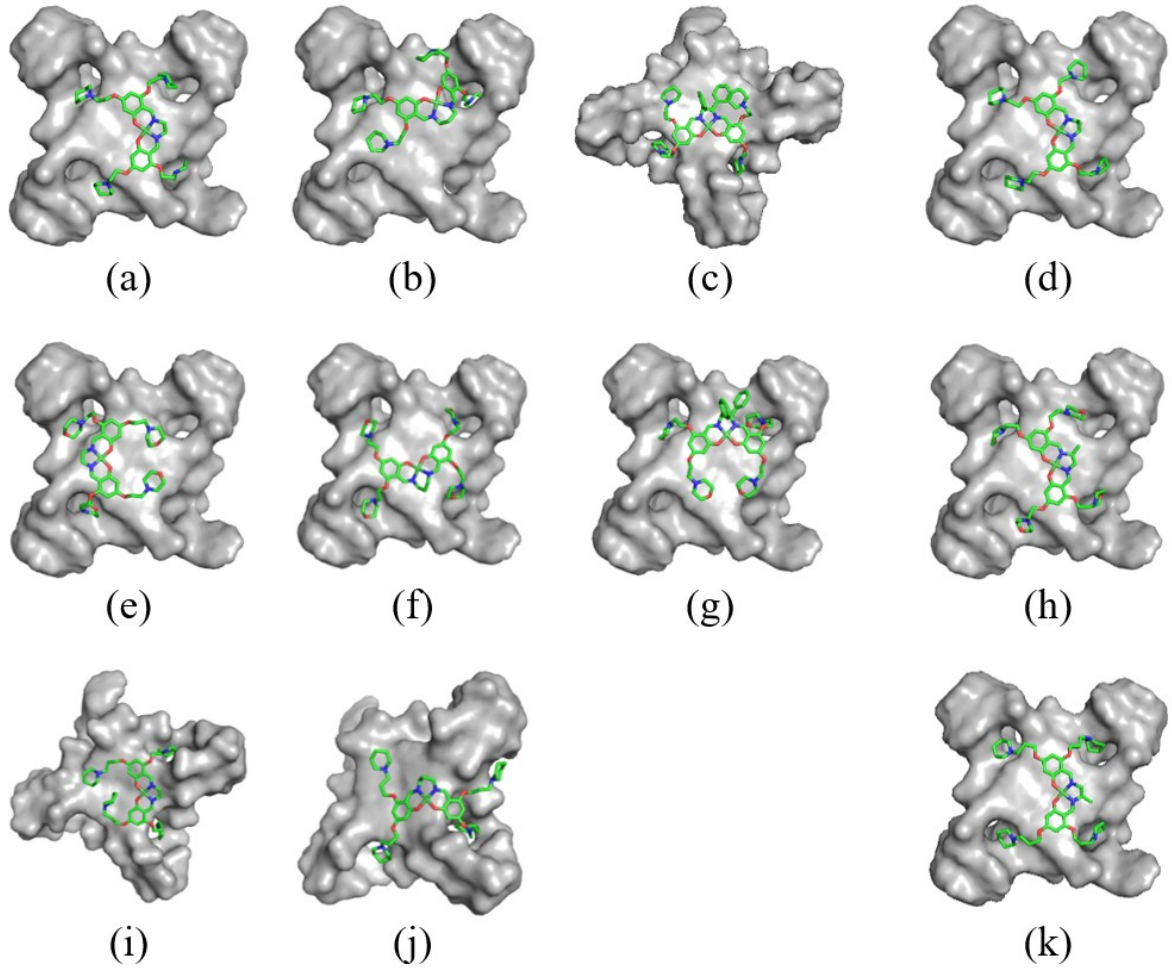

Figure S17: Results from molecular docking experiments performed using the unimolecular G-quadruplex 1KF1 and different nickel complexes: (a) **(7)**; (b) **(10)**; (c) **(13)**: (d) **(15)**; (e) **(8)**; (f) **(11)**; (g) **(14)**; (h) **(16)**; (i) **(9)**; (j) **(12)** and (k) **(17)**.

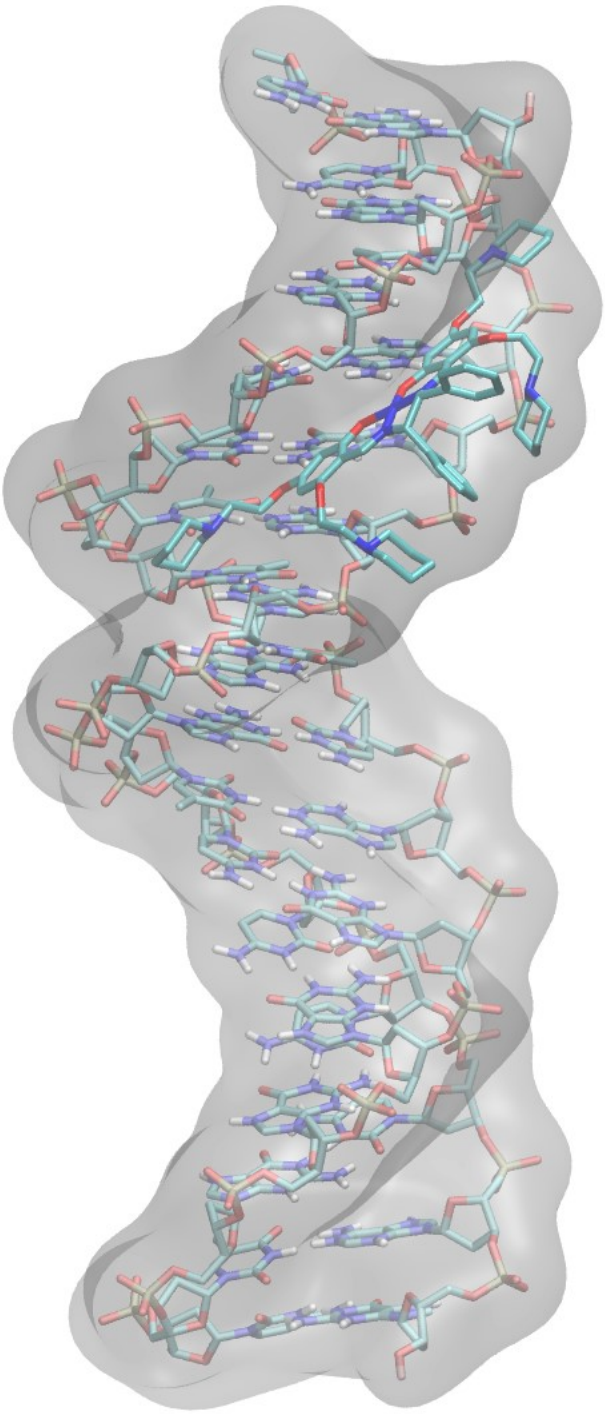

Figure S18(a): High resolution image obtained from molecular docking study involving Ni**(13)** and 1KBD.

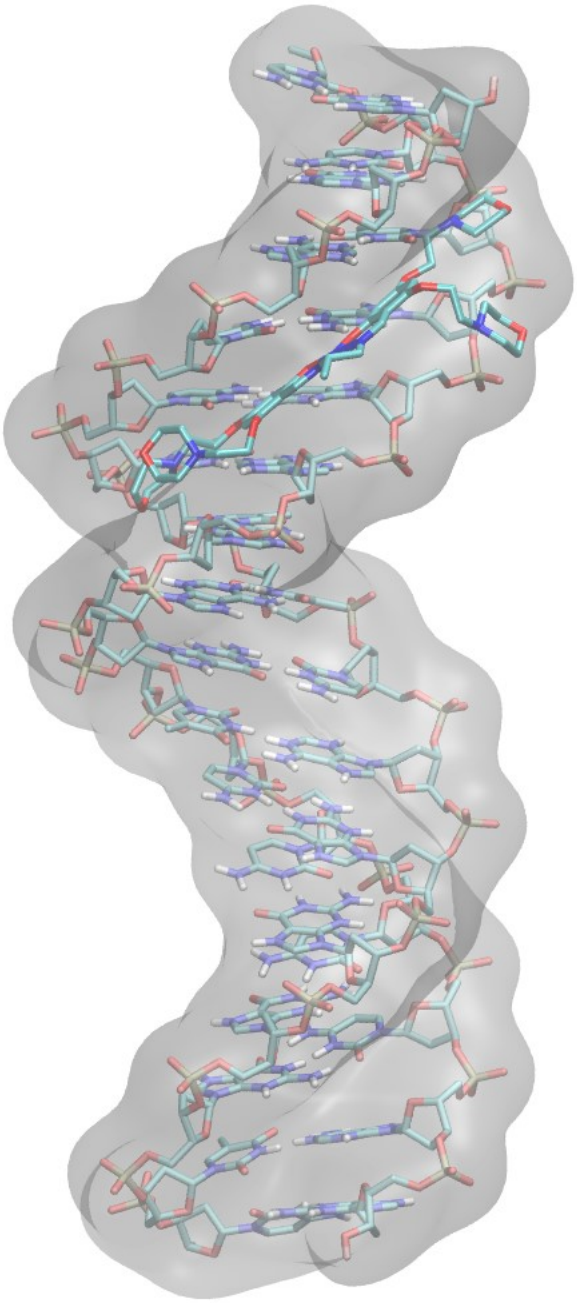

Figure S18(b): High resolution image obtained from molecular docking study involving Ni**(16)** and 1KBD.

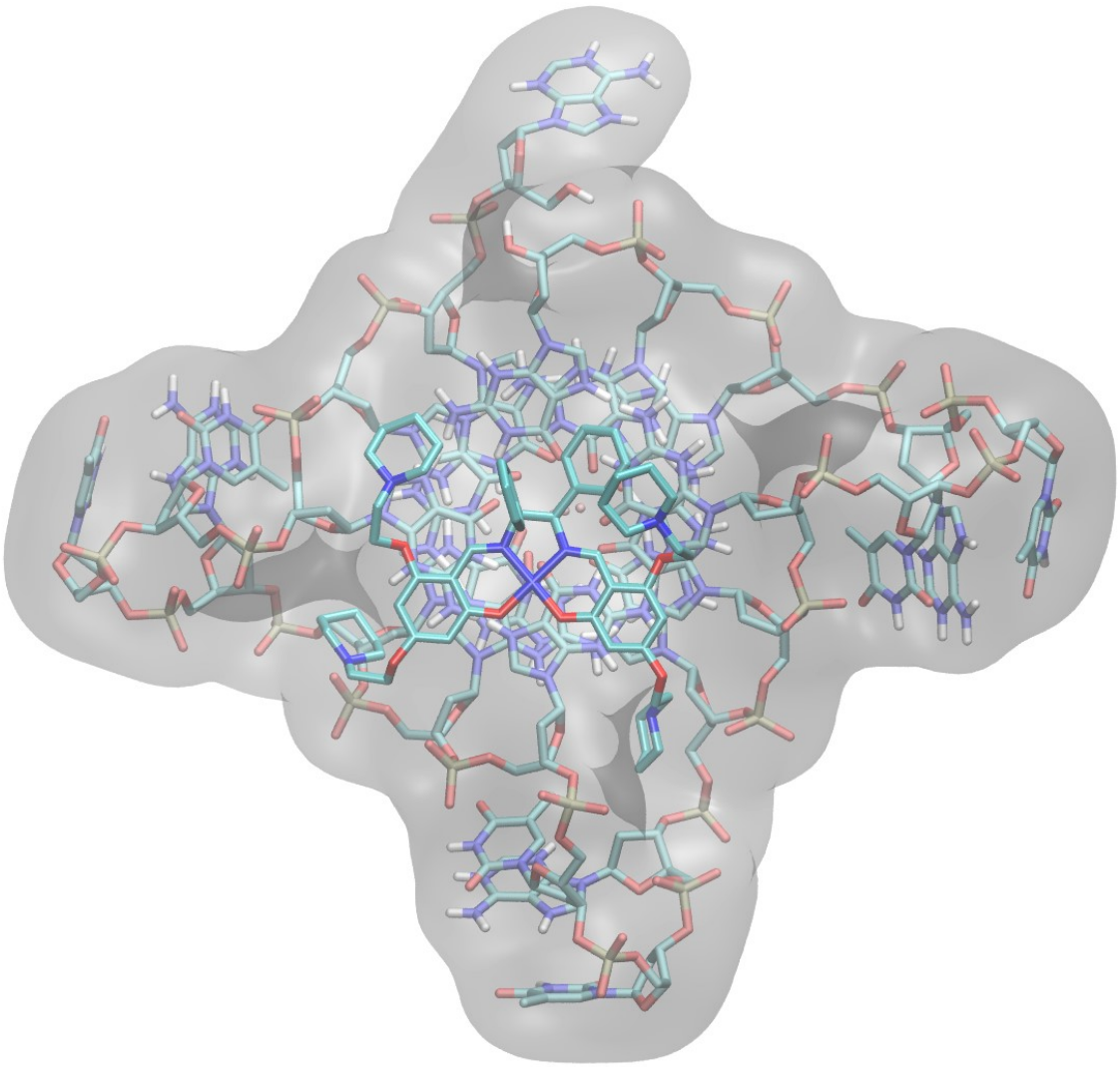

Figure S18(c): High resolution image obtained from molecular docking study involving Ni**(13)** and 1KF1. Orientation 1.

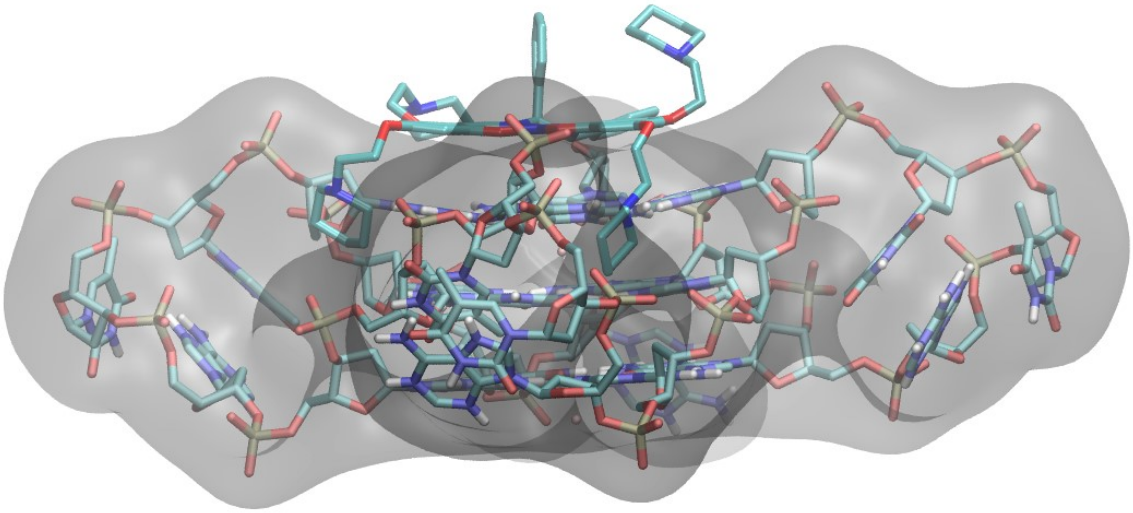

Figure S18(d): High resolution image obtained from molecular docking study involving Ni**(13)** and 1KF1. Orientation 2.

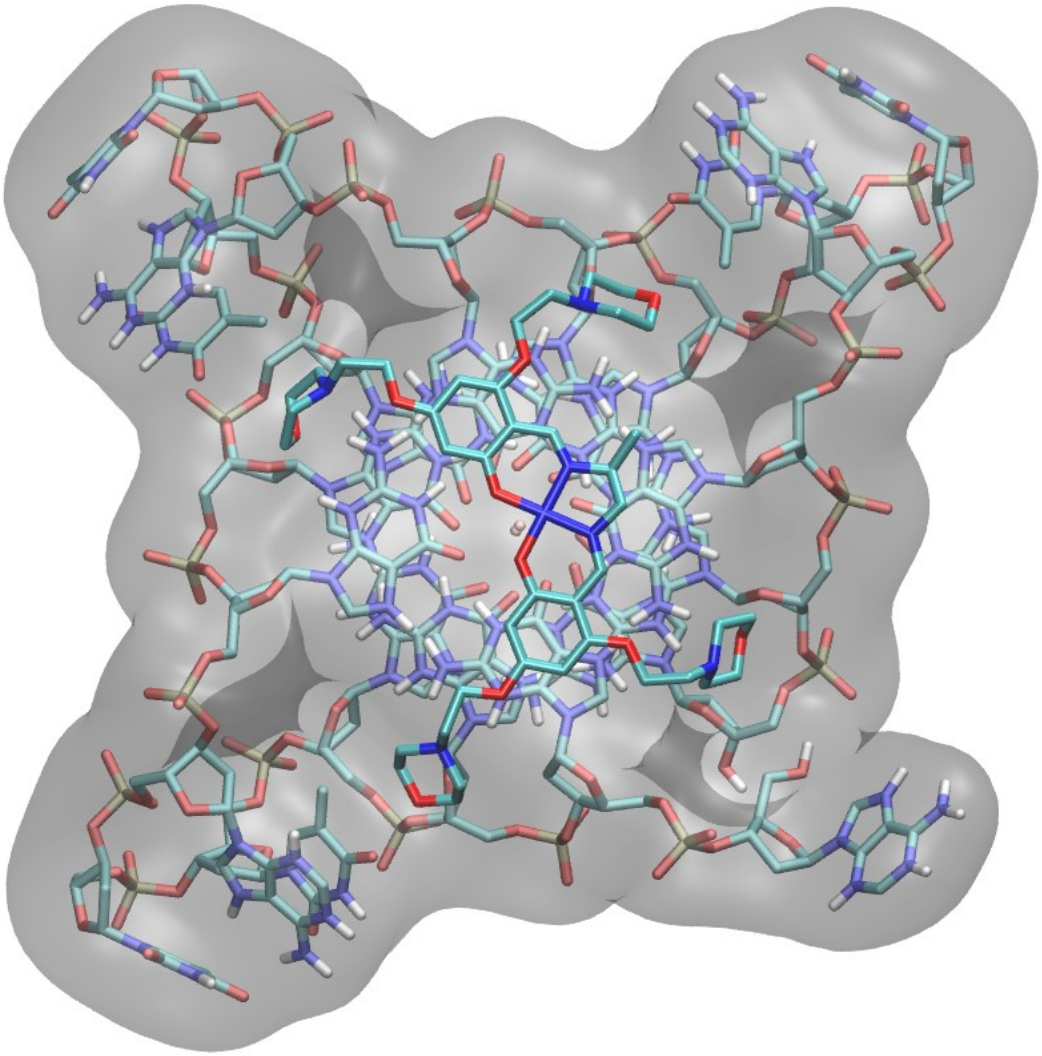

Figure S18(e): High resolution image obtained from molecular docking study involving Ni**(16)** and 1KF1. Orientation 1.

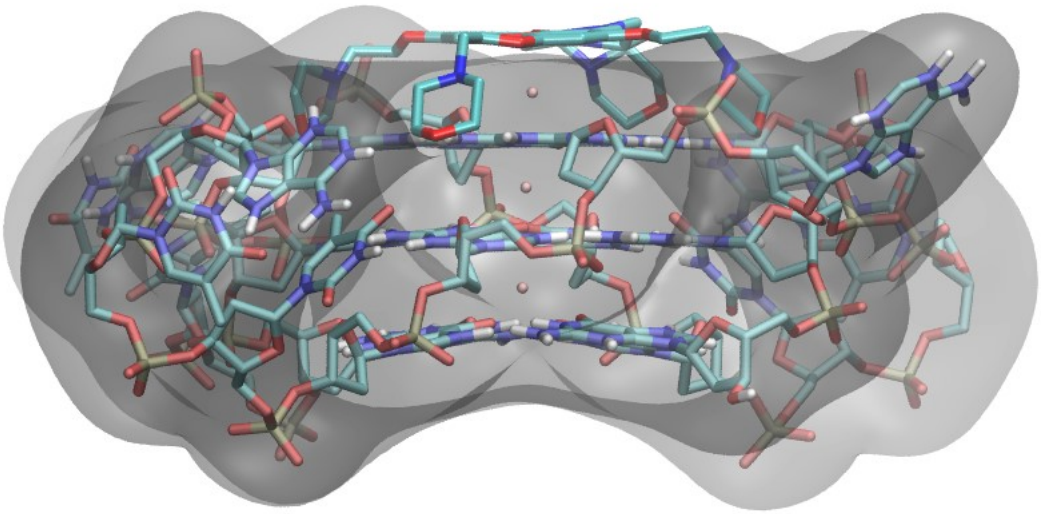

Figure S18(f): High resolution image obtained from molecular docking study involving Ni**(16)** and 1KF1. Orientation 2.

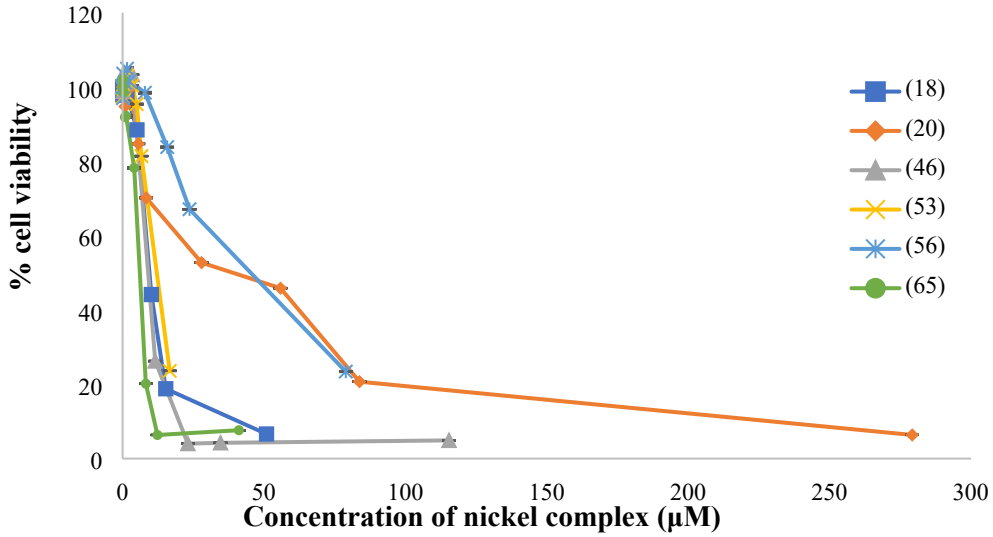

Figure S19: Concentration-response curves obtained from 24 h MTT assays performed using V79 Chinese hamster lung cancer cells and different nickel complexes.

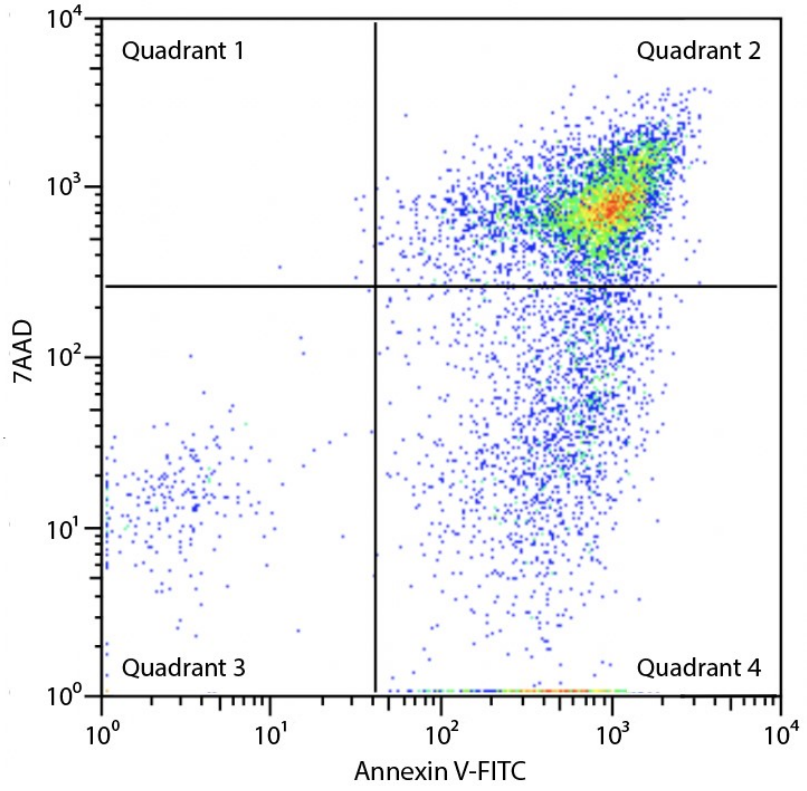
Quadrant 1
Quadrant 2
Quadrant 3
Quadrant 4
7AAD
Annexin V-FITC
10^0
10^1
10^2
10^3
10^4

(a)

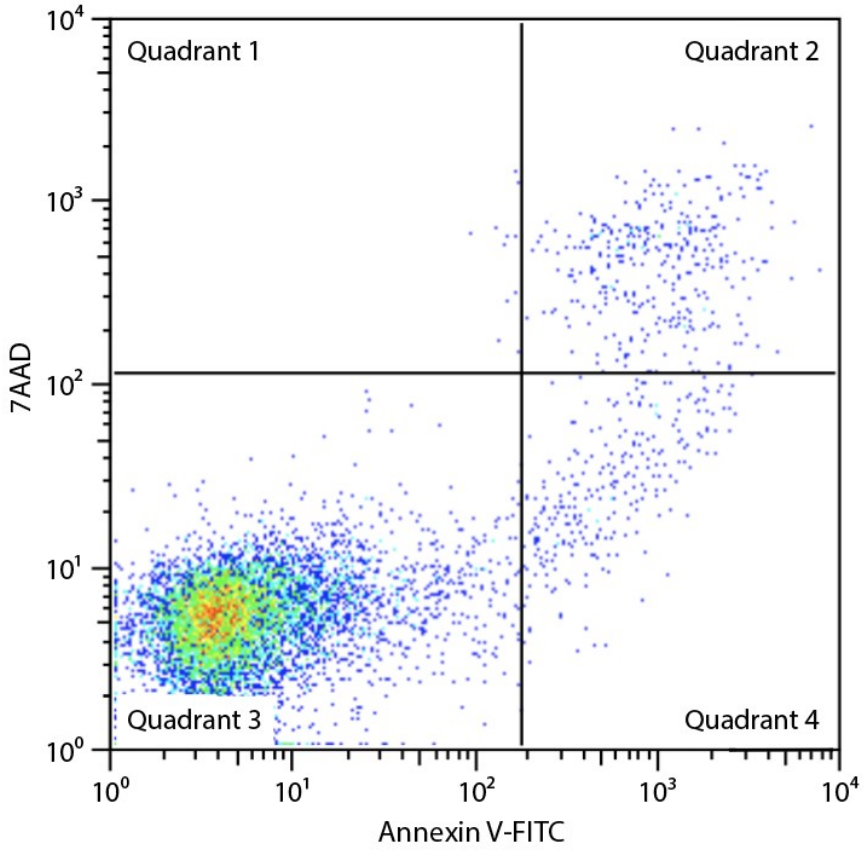
Quadrant 1
Quadrant 2
Quadrant 3
Quadrant 4
7AAD
Annexin V-FITC
10^0
10^1
10^2
10^3
10^4

(b)

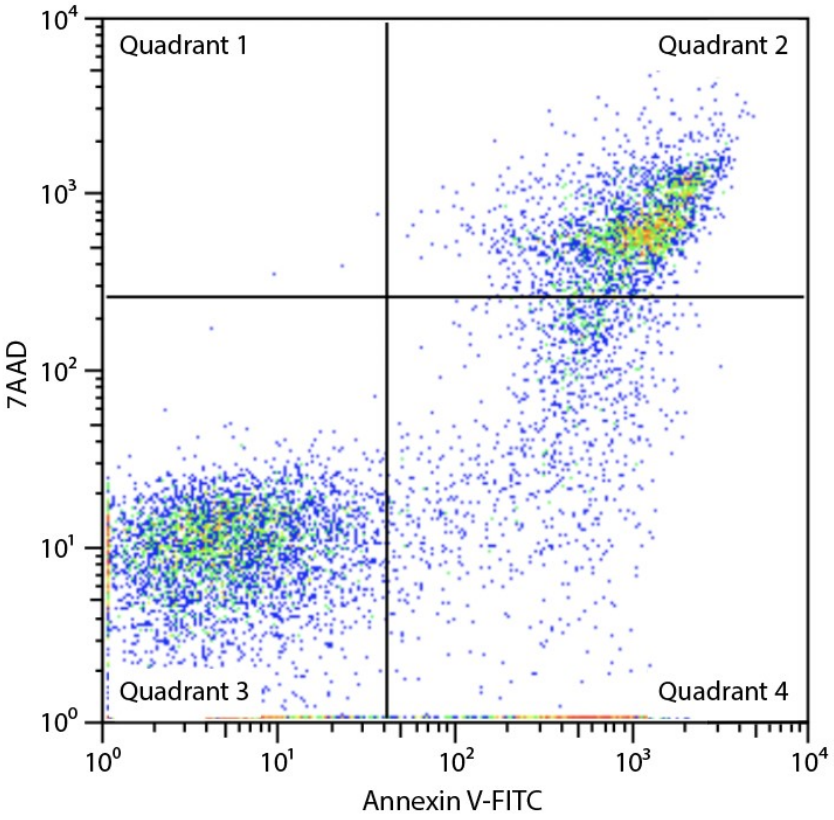

(c)

Figure S20: Results obtained from flow cytometry experiments performed by exposing THP-1 leukemia cells to 10.0 μM nickel complexes for 24 h. The experiments were conducted using Annexin V-FITC and 7AAD fluorescent stains and by collecting 10,000 events. (a) **(18)**; (b) **(19)** and (c) (**21)**.

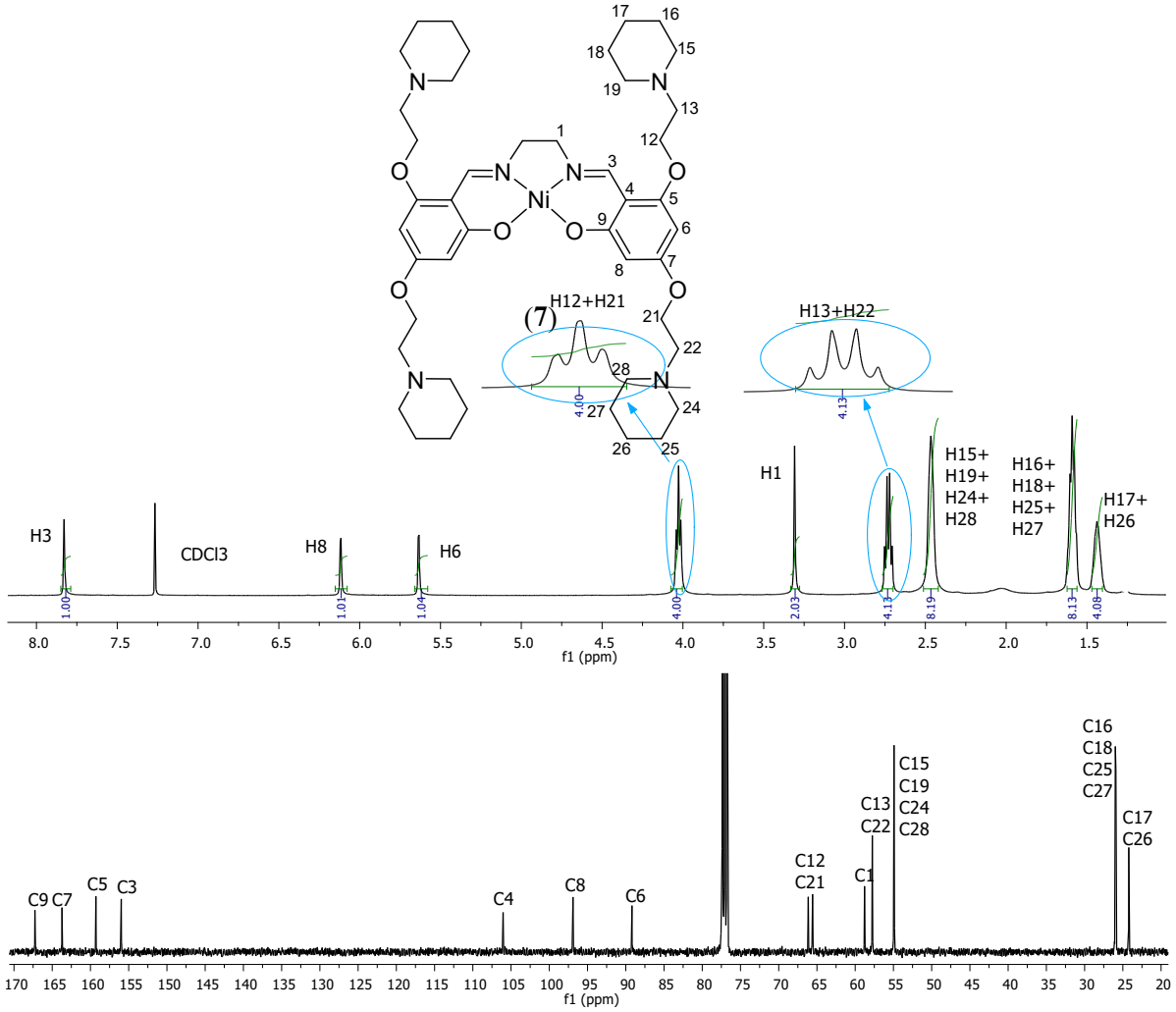

Figure S21: ^{1}H and ^{13}C NMR spectra of (**7**), with expansions of some signals, for clarity.

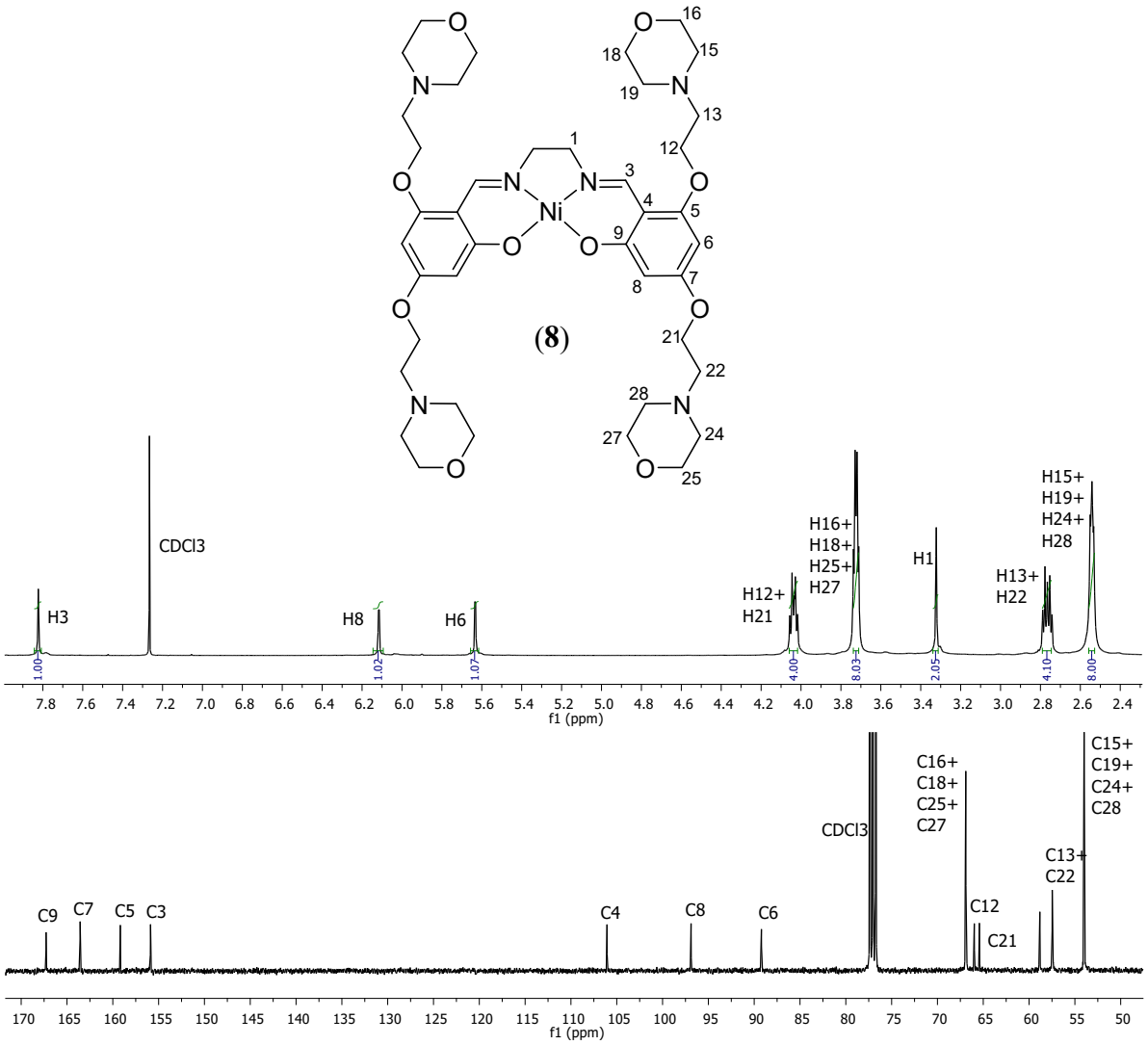

Figure S22: ^{1}H and ^{13}C NMR spectra of (**8**), with expansions of some signals, for clarity.

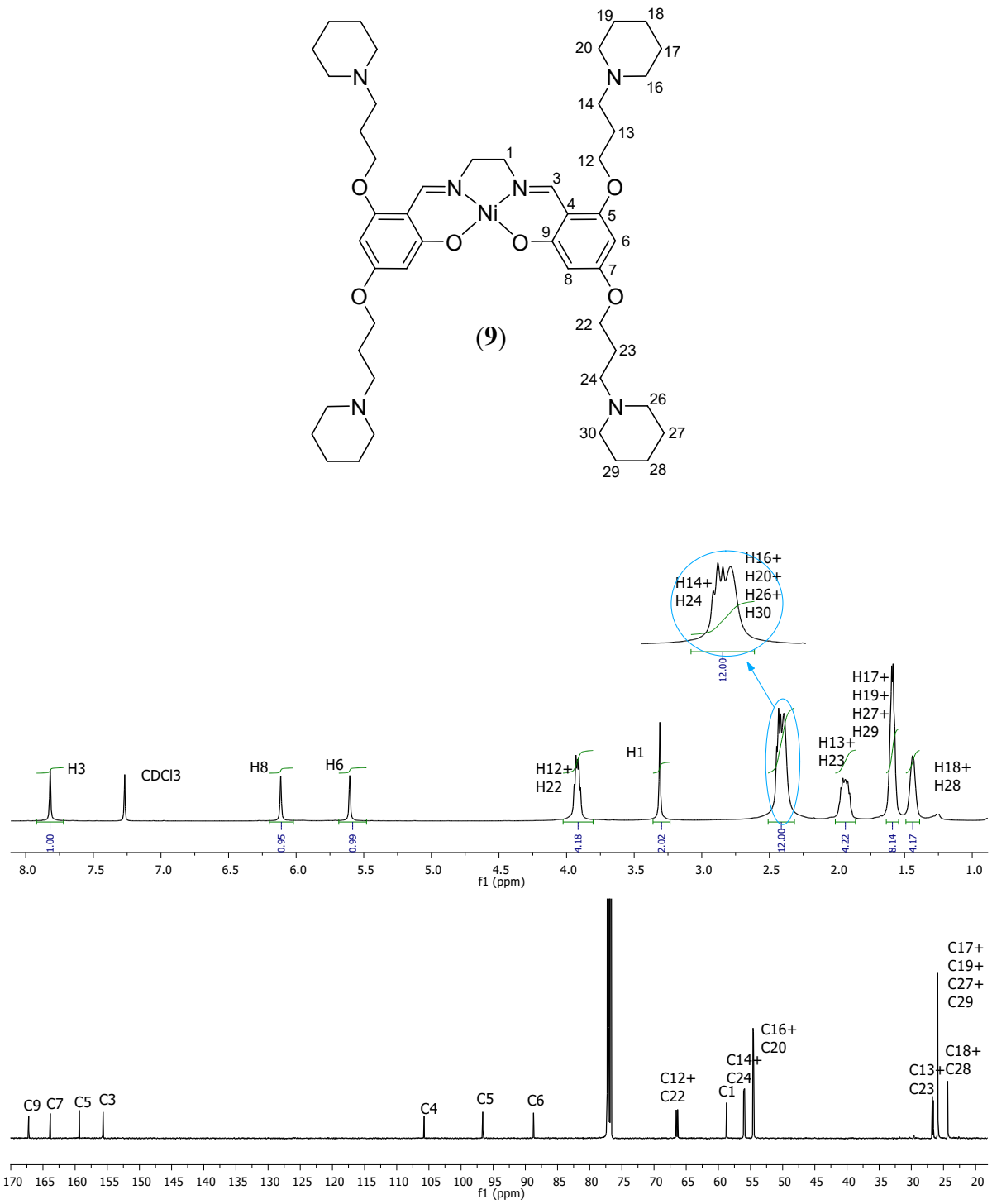

Figure S23: ^{1}H and ^{13}C NMR spectra of (**9**), with expansions of some signals, for clarity.

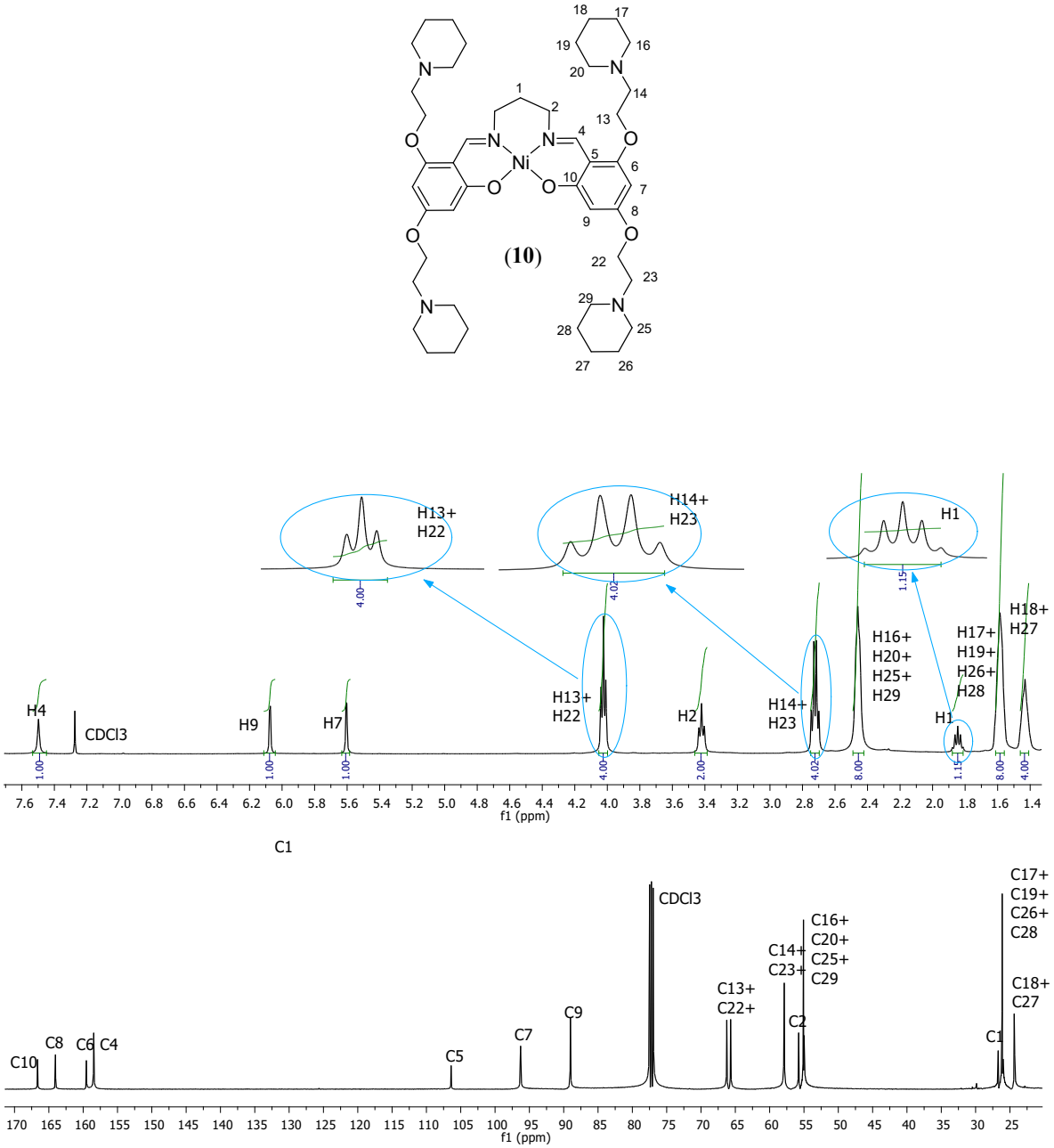

Figure S24: ^{1}H and ^{13}C NMR spectra of (**10**), with expansions of some signals, for clarity.

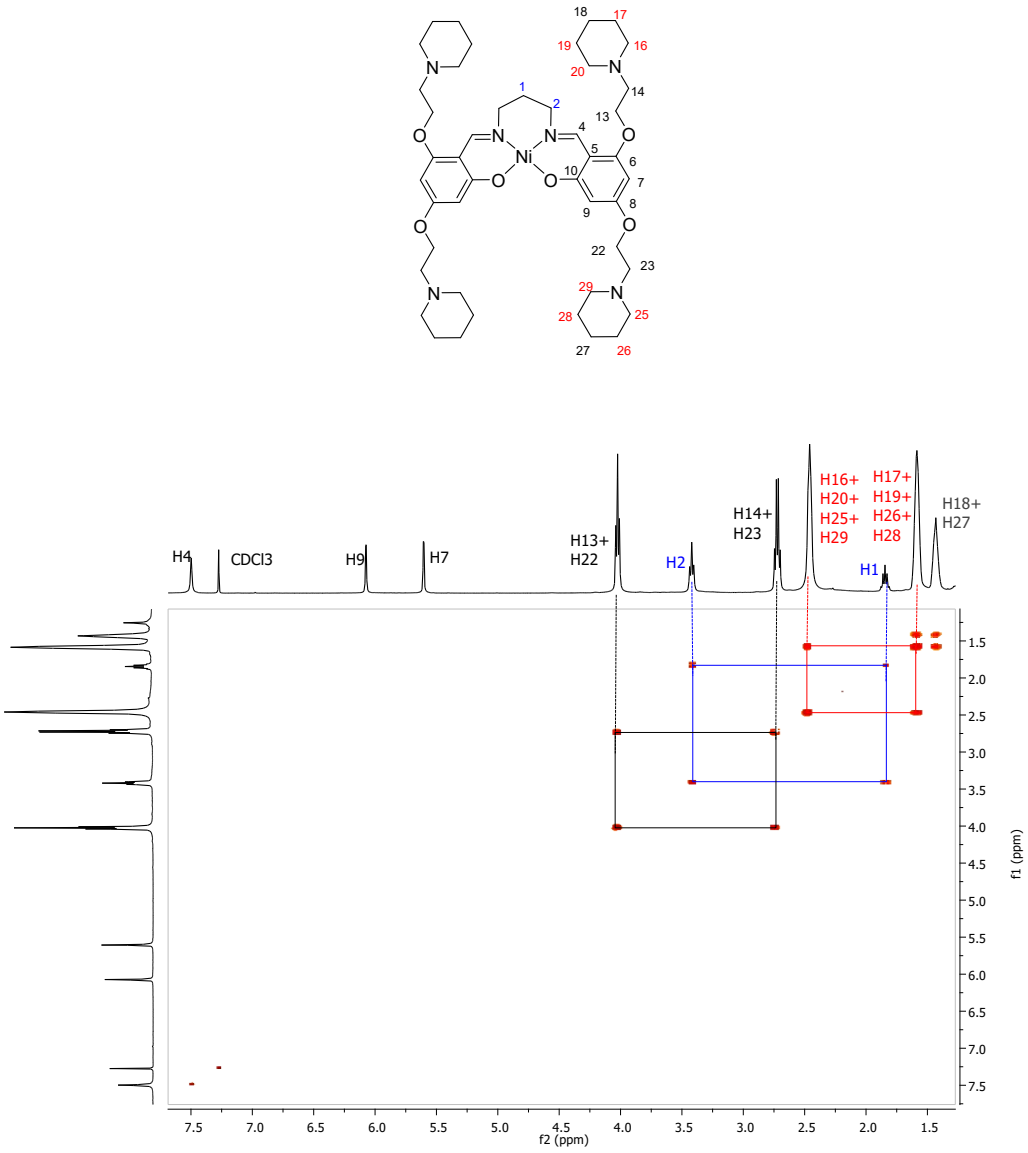

Figure S25: gCOSY spectrum of (**10**), with selected H-H correlations highlighted.

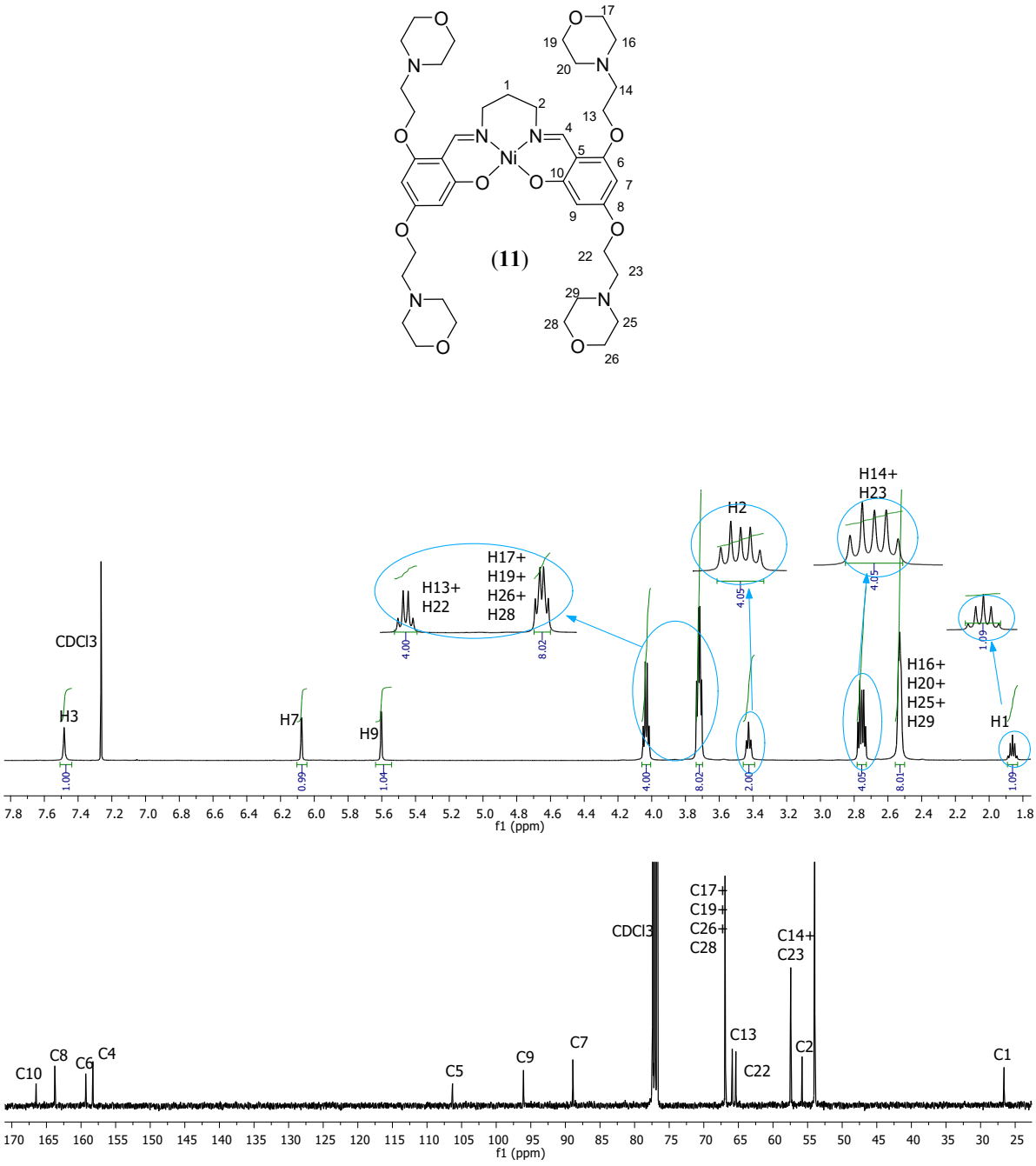

Figure S26: ^{1}H and ^{13}C NMR spectra of (**11**), with expansions of some signals, for clarity.

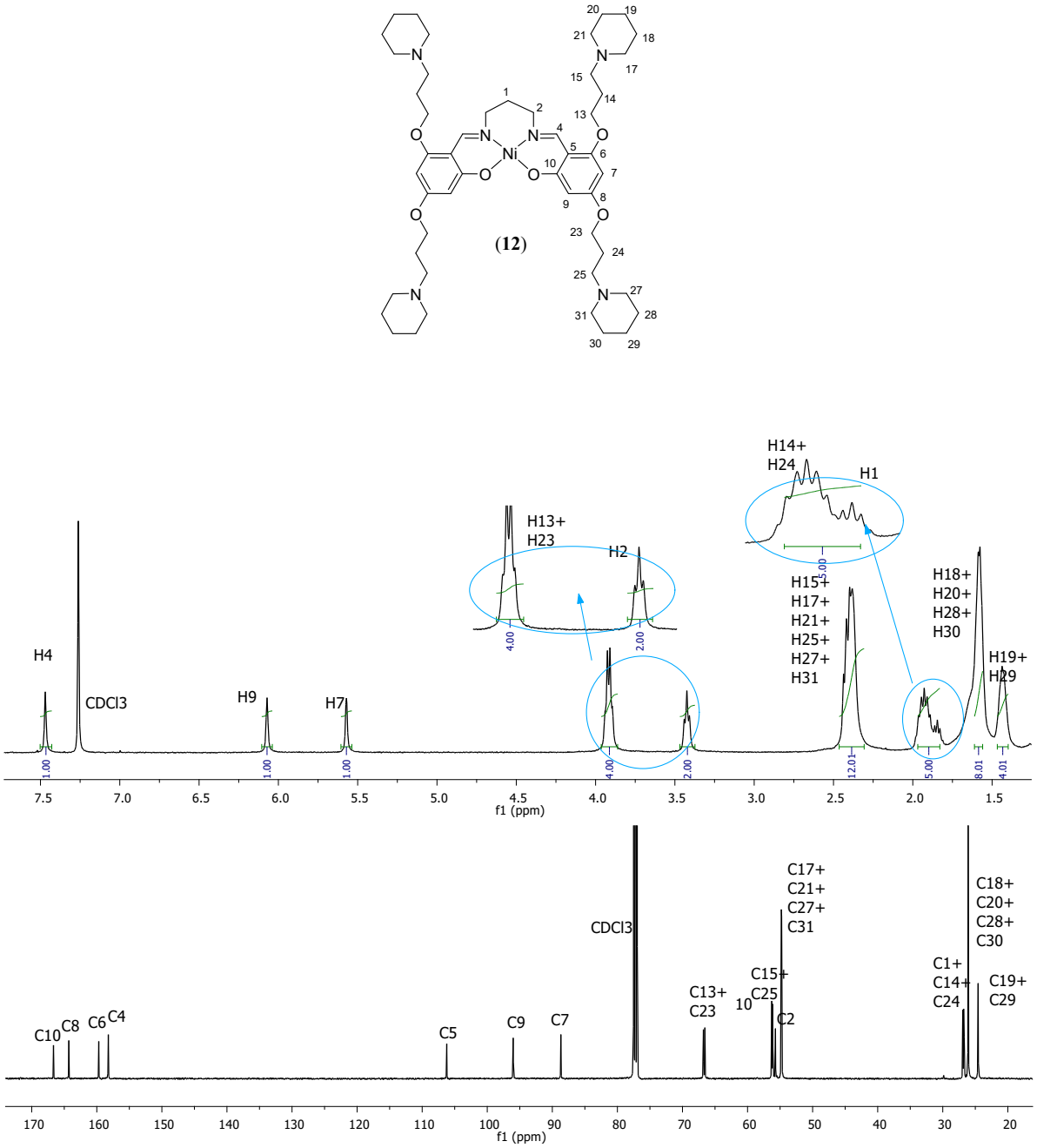

Figure S27: ^{1}H and ^{13}C NMR spectra of (**12**), with expansions of some signals, for clarity.

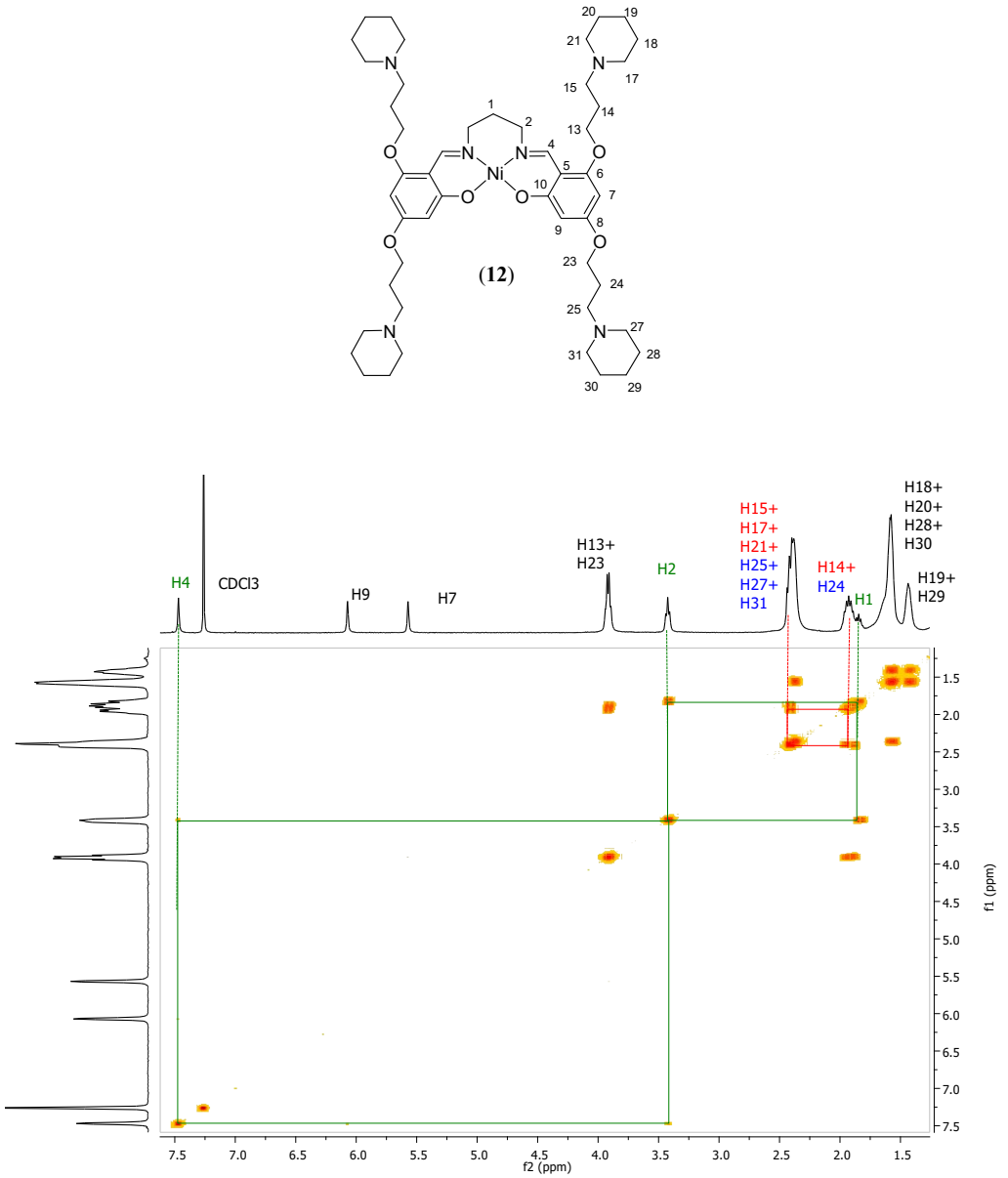

Figure S28: gCOSY spectrum of (**12**), with selected H-H correlations highlighted.

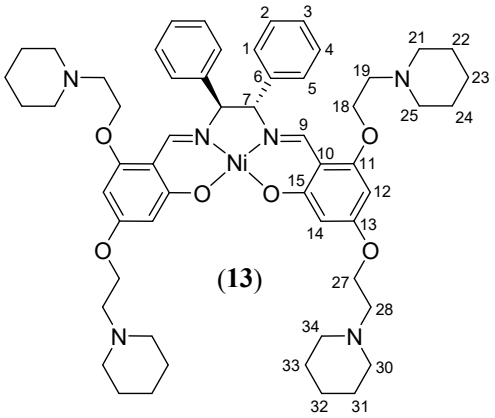

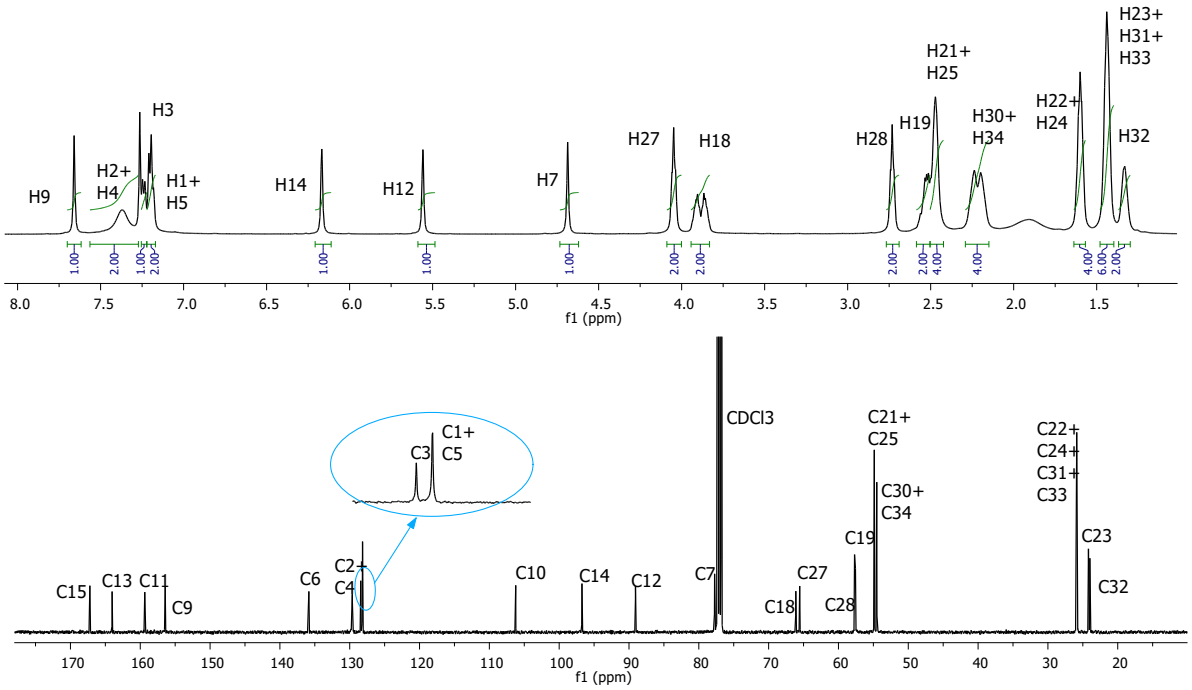

Figure S29: ^{1}H and ^{13}C NMR spectra of (**13**), with expansions of some signals, for clarity.

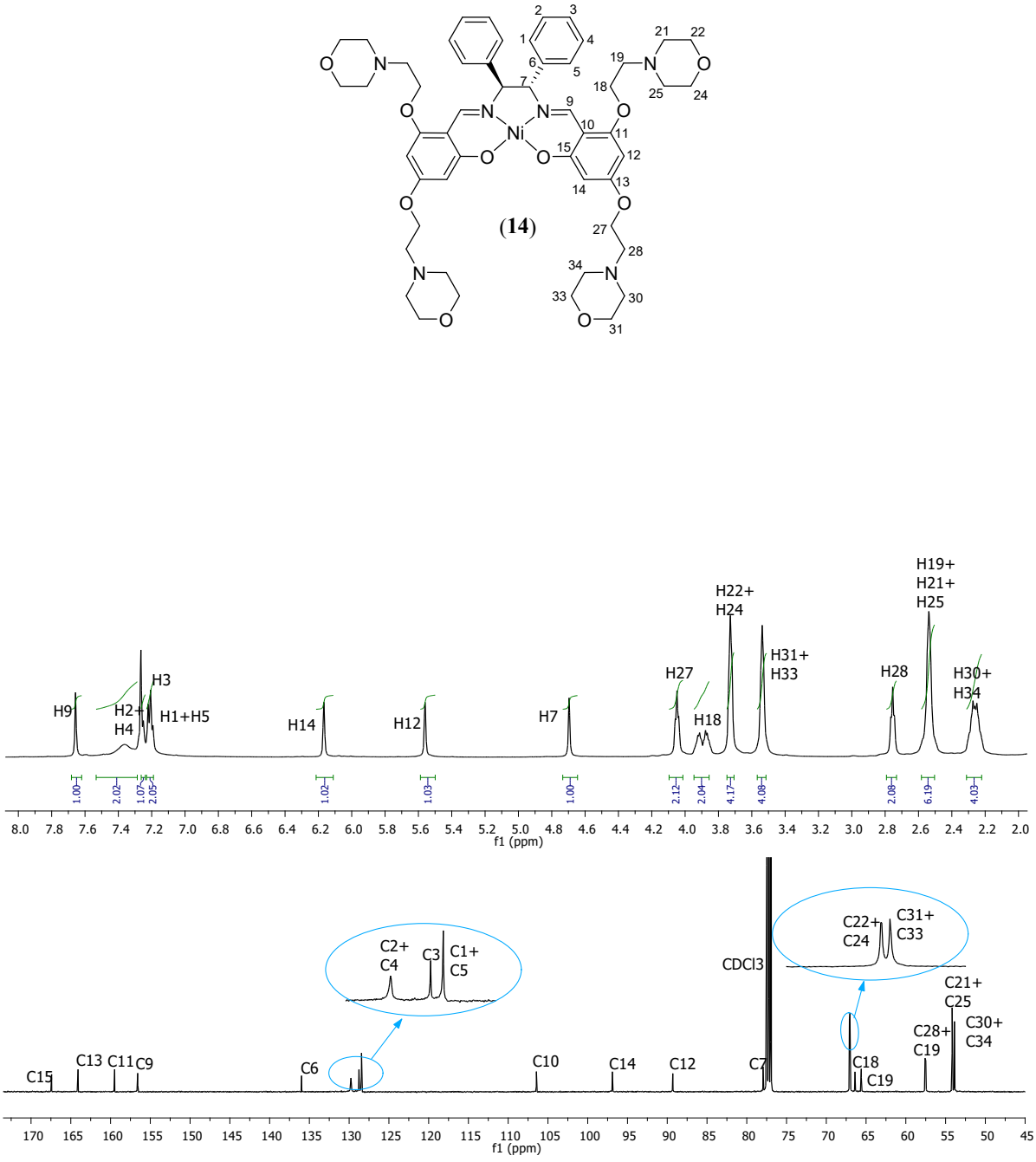

Figure S30: ^{1}H and ^{13}C NMR spectra of (**14**), with expansions of some signals, for clarity.

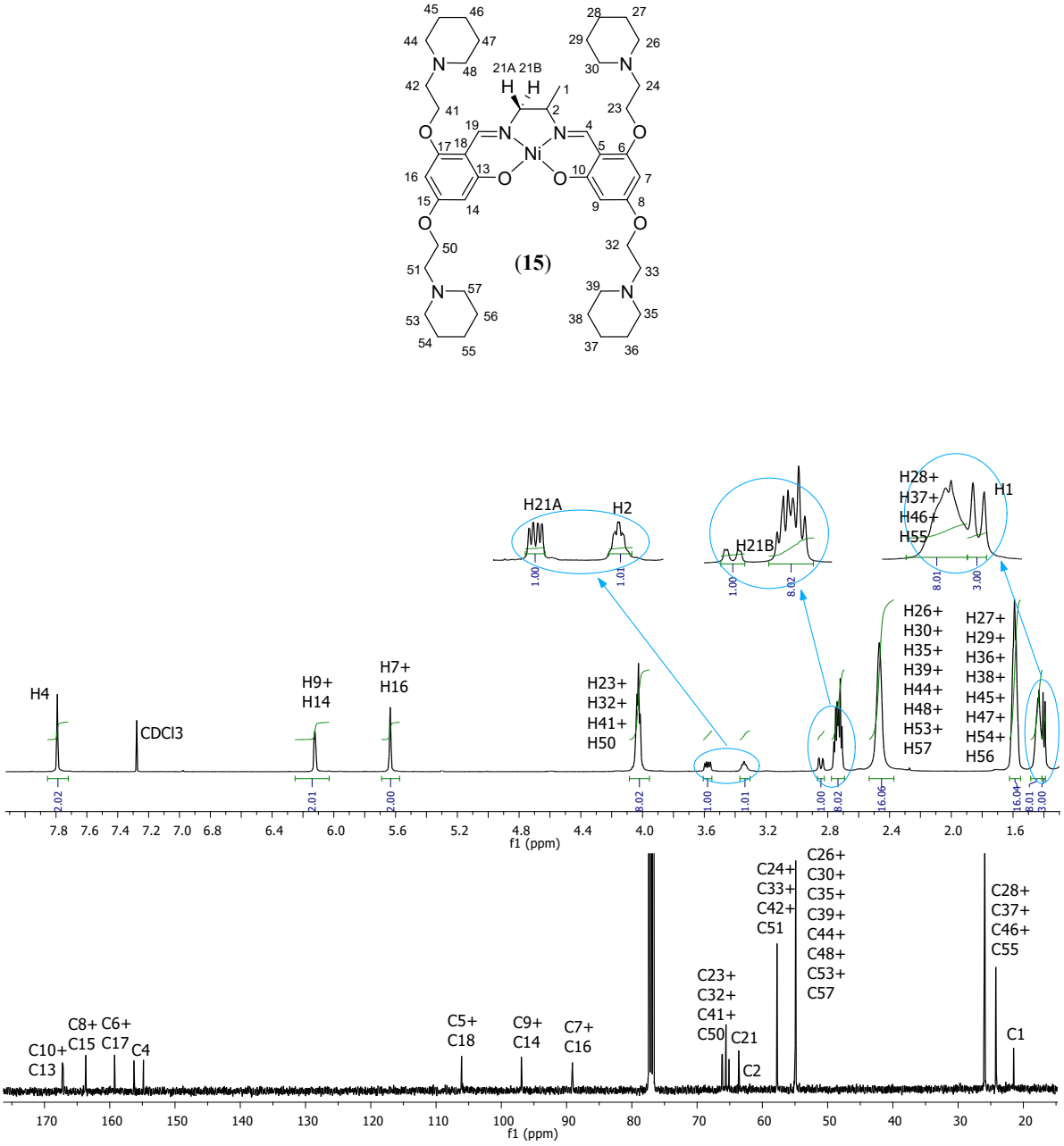

Figure S31: ^{1}H and ^{13}C NMR spectra of (**15**), with expansions of some signals, for clarity.

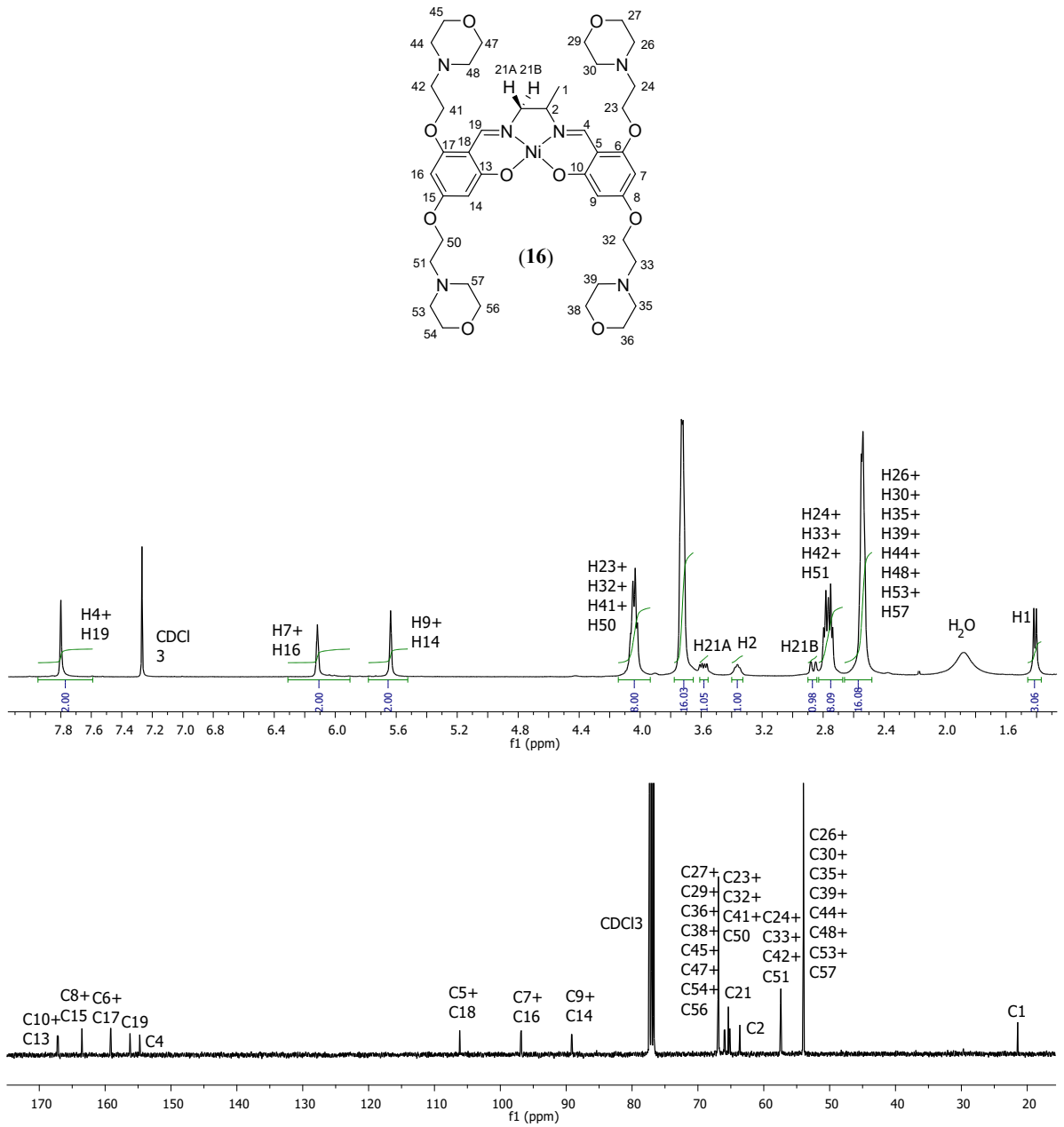

Figure S32: ^{1}H and ^{13}C NMR spectra of (**16**), with expansions of some signals, for clarity.

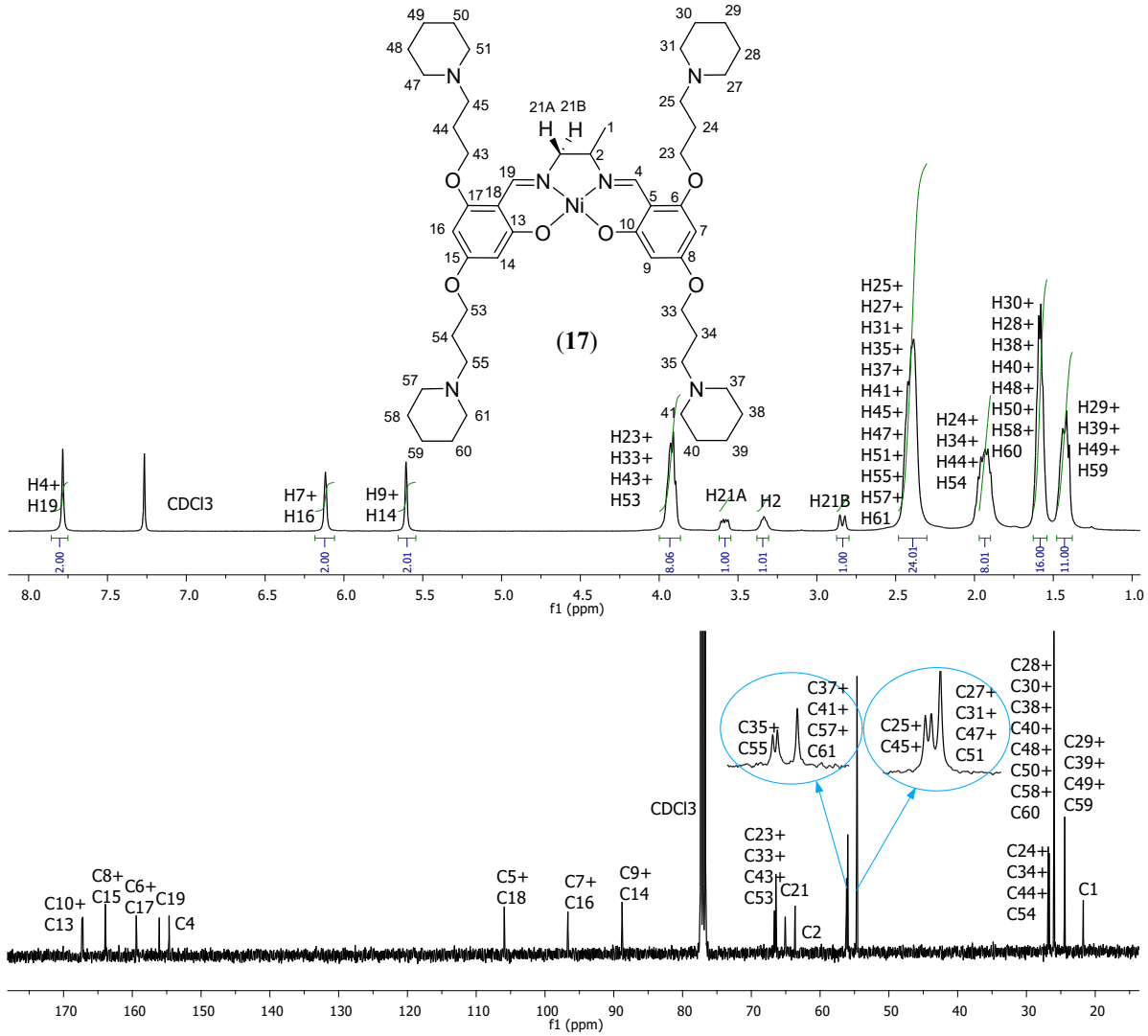

Figure S33: ^{1}H and ^{13}C NMR spectra of (**17**), with expansions of some signals, for clarity.